Barite from the Saf'yanovka VMS deposit (Central Urals) and Semenov-1 and -3 hydrothermal sulfide fields (Mid-Atlantic Ridge): A comparative analysis of formation

Barite from the Saf'yanovka VMS deposit (Central Urals) and Semenov-1 and -3 hydrothermal sulfide fields (Mid-Atlantic Ridge): A comparative analysis of formation conditions

Nataliya P. Safina • Irina Yu. Melekestseva • Paolo Nimis • Nataliya N. Ankusheva • Anatoly M. Yuminov • Vasily A. Kotlyarov • Sergey A. Sadykov

N. P. Safina, I. Yu. Melekestseva (corresponding author), N.N. Ankusheva, V.A. Kotlyarov, S.A. Sadykov
Institute of Mineralogy, Urals Branch of Russian Academy of Sciences
Miass, Chelyabinsk District
456317 Russia
e-mail: safina@ilmeny.ac.ru

I. Yu. Melekestseva
e-mail: melekestseva-irina@yandex.ru

N.N. Ankusheva
e-mail: ankusheva@ilmeny.ac.ru

V.A. Kotlyarov
e-mail: kotlyarov@mineralogy.ru

S.A. Sadykov
e-mail: sadykov@mineralogy.ru

P. Nimis
Dipartimento di Geoscienze, Università degli Studi di Padova
Via Gradenigo 6
35131 Padova, Italy
e-mail: paolo.nimis@unipd.it

N. P. Safina, N.N. Ankusheva, A.M. Yuminov
Faculty of Geology, South-State Urals University
8 Iyulya st. 10., Miass, Chelyabinsk District
456301 Russia

A.M. Yuminov
e-mail: umin@mineralogy.ru

Key words: barite, Central Urals, fluid inclusions, hydrothermal sulfide field, mid-Atlantic Ridge, sulfur isotopic compositions, VMS deposit

Abstract

Hydrothermal and diagenetic barites from colloform and clastic pyrite–rich ores from the weakly metamorphic Saf'yanovka volcanogenic massive sulfide deposit (Devonian, Central Urals) were studied in comparison with barite from similar modern seafloor deposits from the mid-Atlantic Ridge (Semenov-1 and Semenov-3 hydrothermal fields). Hydrothermal barites from all the studied deposits exhibit similar morphology: they occur as tabular crystals or their aggregates. In contrast, diagenetic barite from clastic ores of the Saf'yanovka deposit occur as compact aggregates of deformed, broken, or slightly curved tabular crystals with stylolite boundaries. The variable Sr contents in the studied barites show no relationship with the genetic types. The average $\delta^{34}S$ values of hydrothermal barite from both ancient and modern colloform sulfides (+22.9 ‰, Saf'yanovka deposit; +21.2‰, Semenov-1 field) match those of Silurian–Devonian and contemporary seawater, respectively. The lower $\delta^{34}S$ of hydrothermal barite from clastic sulfides of the Semenov-3 field (+19.6 ‰), which is associated with high-Se, high-temperature chalcopyrite, indicates light sulfur contribution from oxidation of fluid H_2S. The higher average $\delta^{34}S$ of diagenetic barite from clastic

ores of the Saf'yanovka deposit (+28.1‰) is interpreted to reflect partial thermochemical reduction of seawater sulfate due to interaction with ferrous minerals and/or organic matter.

In spite of different geodynamic setting, hydrothermal barite from colloform ores from the Saf'yanovka deposit (back-arc basin) and Semenov-1 field (slow-spreading mid-oceanic ridge) were formed under similar low- to moderate-temperature conditions (172–194 °C and 83–233 °C, respectively) from relatively low-salinity fluids (1.6–4.5 and 0.6–3.8 wt.% $NaCl_{eq}$, respectively). Variations in salinity values from higher- to lower-than seawater reflect phase separation in the parent fluids. High contents of CO_2, CH_4, and N_2 (up to 1.58, 0.05, and 0.006 mol%, respectively) in fluid inclusions from the Saf'yanovka deposit are attributed to reactions with abundant hydrothermal fauna and C-bearing sediments. The presence of SO_2 and CO_2 in fluid inclusions from the Semenov-1 field is ascribed to contributions from a magmatic fluid. Hydrothermal barite from Semenov-3 clastic sulfides crystallized at higher-temperature (266–335 °C) from higher-salinity fluids (4.8–9.2 wt.% $NaCl_{eq.}$). The high salinity may again indicate a contribution from a magmatic fluid, consistent with high measured CO_2 content in fluid inclusions (1.6 mol%). Diagenetic barite from the Saf'yanovka clastic ores was formed at moderate temperatures (140–180 °C) from low- to moderate-salinity pore fluids (1.4–5.4 wt.% $NaCl_{eq.}$). The variable salinity may reflect contributions from various water sources, e.g., connate seawater, silicate dehydration, and transformation of primary hydrothermal barite with low-salinity fluid inclusions.

Combining our new data with those for other seafloor hydrothermal barites the following systematics can be defined. Barite precipitated on chimney rims or associated with pyrite-rich, colloform, massive sulfides forms at relatively low to moderate temperatures (<230 °C), barite associated with polymetallic-rich sulfides forms at moderately high temperatures (210–280 °C), and barite in assemblage with chalcopyrite records the highest temperatures (265–335 °C). The main source of sulfur is seawater for both hydrothermal and diagenetic barite; additional contribution of isotopically light sulfur from partial oxidation of H_2S or of isotopically heavy sulfur from bacterial sulfate reduction may occur in hydrothermal barite, whereas a contribution from isotopically heavy sulfur remaining after thermochemical or bacterial partial reduction of seawater sulfate appears to be common in diagenetic barite.

Introduction

Barite may form in seafloor environments by a number of processes, such as (i) hydrogenetic precipitation from the water column (i.e., 'marine' barite), (ii) diagenetic precipitation from pore fluids in sediments, (iii) precipitation from cold seeps, and (iv) precipitation from low-temperature (<120 °C) to high-temperature (>300 °C) hydrothermal fluids venting on the seafloor in various geodynamic settings (e.g., Sasaki et al. 1995; Hou et al. 2001; Paytan et al. 2002; de Ronde et al. 2003; Petersen et al. 2004; Hein et al. 2007; Griffith and Paytan 2012). The conditions of formation of seafloor barite are recorded in its habit, chemical and isotopic composition, and fluid inclusions (Paytan et al. 2002). Barite is a common gangue mineral in both modern seafloor sulfide-rich, hydrothermal vent systems and in their ancient counterparts, which are represented by on-land, volcanic-hosted massive sulfide (hereafter, VMS) deposits. The direct comparison of barite in ancient and modern hydrothermal systems can be difficult because the primary hydrothermal features of ancient deposits are often modified by later metasomatic or metamorphic processes.

In this paper, we compare barite in colloform and clastic pyrite-rich ores from the Paleozoic Saf'yanovka VMS deposit, Central Urals (Fig. 1), with barite in colloform and clastic pyrite-rich ores from the modern Semenov-1 and -3 hydrothermal fields, Mid-Atlantic Ridge (hereafter, MAR) (Fig. 2). In spite of their different geodynamic setting (back-arc spreading center for the Saf'yanovka deposit, cf. Yazeva et al., 1991, vs mid-oceanic ridge for the Semenov-1 and -3 hydrothermal fields, Beltenev et al., 2007), these deposits were chosen for their significant similarities of pyrite-rich ores in terms of textures and mineral assemblages, characterized by predominance of iron disulfides and presence of abundant barite. Moreover, the weakly metamorphic character of the Saf'yanovka deposit, which allowed preservation of its delicate primary hydrothermal structures (uncommon for Paleozoic VMS deposits, which are often modified by later metasomatism or metamorphism), enabled a detailed comparison with its modern counterparts. By comparing previous data for barite from these deposits with our newly acquired geochemical, isotopic and fluid inclusion data and with published data on other ancient and modern seafloor hydrothermal deposits, we will investigate the major distinctive features of different types of barites (hydrothermal vs. diagenetic) and the systematics between temperatures of barite formation and mineralogy and textures of associated sulfides.

Geological outlines of the studied deposits

Saf'yanovka deposit

The Saf'yanovka massive sulfide deposit, discovered in 1985, is situated in the Sverdlovsk district, 9 km northeast of the town of Rezh in the Central Urals (Fig. 1a). The deposit is located in the East Uralian megazone, in the Rezh ore district. The geological setting, host rocks, and ore mineralogy of the Saf'yanovka deposit have been studied in detail and are described in Yazeva et al. (1991), Koroteev et al. (1997), Maslennikov (2006), Maslennikova and Maslennikov (2007), Safina and Maslennikov (2009), Soroka et al. (2010), Murzin et al. (2010), Chuvashov et al. (2011), and Yaroslavtseva et al. (2012). The deposit is thought to have formed in a Devonian back-arc basin which hosts a rhyolite–dacite–andesite–basalt association (Yazeva et al. 1991; Koroteev et al. 1997). The area of the deposit consists of a stack of three main tectonic slivers; (i) a ~50 m-thick lower sliver composed of Late Devonian basalts and basaltic andesites, (ii) a ~500 m-thick ore-hosting middle sliver composed of Middle Devonian dacites and rhyolites, interlayered with volcano-sedimentary rocks and black shales, and (iii) an upper sliver, up to 300 m-thick, composed of Middle Devonian serpentinites, gabbro, limestones and basalts, interlayered with Upper Devonian–Lower Carboniferous cherts (Fig. 1b; Yazeva et al. 1991; Koroteev et al. 1997).

The deposit includes ten ore lenses up to 40 m-thick, which occur in three stratigraphic horizons at depths of 190 to 400 m. In the central part of the deposit, the sulfide bodies are separated by volcano-sedimentary layers ranging in thickness from several cm to over 10 m. At their margins, the sulfide bodies are alternated with black shales (C_{org} 2.7–3.5 wt%) up to 5 m-thick (Yaroslavtseva et al. 2012). A 5–7 m-thick zone of nearly monomineralic barite lies directly beneath the ore bodies, at a depth of about –200 m.

The main ore body exposed by the open pit is up to 200 m thick and is split on its flanks into several segments by subvolcanic rhyolite bodies (Fig. 1b; Yazeva et al. 1991; Koroteev et al. 1997). A few barite–sphalerite layers with thicknesses of about one meter occur on the southern margin of the main ore body. The deposit is remarkable considering the low degree of metamorphism (lower greenschist facies) of the host rocks and massive sulfide ores (Yazeva et al. 1991), which allowed preservation of delicate primary structures such as fine-grained colloform ores, black-smoker chimneys, and fossilized hydrothermal fauna (Maslennikov 2006; Maslennikova and Maslennikov 2007). The sulfide ores include several types: massive Cu–Zn, Cu and Fe ores with dominant, massive, banded and breccia-like structures, stockwork Cu ores consisting of a chalcopyrite-pyrite network in hydrothermally altered volcanic rocks, and Cu–Zn coarse-grained disseminated ores at the contacts with massive ores.

Based on detailed ore-facies mapping, the major, vertical, conical sulfide lens, the core of which is composed of massive Cu–Zn ores with relics of quartz–sphalerite–chalcopyrite black-smoker chimneys, has been interpreted as a remnant sulfide mound (Fig. 1c; Maslennikov 2006). According to the ore-facies reconstruction, colloform pyrite ores with barite and quartz at the top of the sulfide body are thought to represent fragments of seafloor hydrothermal crusts. Sulfide breccias and sandstones with clasts derived from massive and colloform sulfides and black smoker chimneys, cemented by quartz or barite, are widespread on the flanks of the sulfide layers. Stringer–disseminated Cu and Cu–Zn ores, comprising more than half of the reserves of the deposit, are localized beneath the major ore body (Yazeva et al. 1991). Veins composed of coarse-crystalline chalcopyrite and pyrite are fragmented and cemented by quartz and barite.

Preliminary data on homogenization temperatures of fluid inclusions in barite from colloform (160–190 °C) and clastic (130–170 °C) ores and in vein barite in massive ores (160–200 °C) were reported in Safina et al. (2012).

Semenov-1 and Semenov-3 fields

The inactive Semenov-1 and Semenov-3 hydrothermal fields are part of the large Semenov massive sulfide cluster that was discovered in 2007 during the 30th cruise of the Russian R/V *Professor Logachev* by the Polar Marine Geosurvey Expedition (PMGE) in collaboration with VNIIOkeangeologia, Saint Petersburg, Russia (Beltenev et al. 2007). The Semenov cluster is located between the Fifteen Twenty and Marathon transform fracture zones on the western wall of the mid-ocean rift valley, on a EW-trending seamount approximately 10 km-long and 4.5 km-wide (Beltenev et al. 2007; Fig. 2). The substrate of the Semenov cluster is believed to be a detachment fault structure, which exposes deep oceanic basement rocks on the seafloor (Smith et al. 2008; McLeod et al. 2009). The hydrothermal fields of the Semenov cluster are located between depths of 2400 and 2950 m. The large vertical extent of the mineralization is mainly due to the structure of the Semenov-4 field, which is the largest field in the cluster (several square kilometer-wide). This field is characterized by significant post-depositional faulting, which allowed exposure of stockwork veining in substrate basalts (Beltenev et al. 2007; Jamieson et al. 2014).

Serpentinized ultramafic rocks (mainly harzburgites) were recovered from the northern, southern, and western slopes of the seamount (Beltenev et al. 2007; Fig. 2). Other igneous rocks are given by gabbros, olivine gabbros, gabbronorites, ferrogabbros, plagiogranites, tonalites, and diorites. Volcanic and subvolcanic rocks are represented by aphyric and plagiophyric pillow lavas (locally with well-preserved chilled glasses) and dolerites, respectively (Pertsev et al. 2012). Hydrothermal alteration is shown by the formation of serpentinized harzburgites, talcites, chloritized mafic rocks, talc-chlorite rocks, and amphibolites.

The Semenov-1 hydrothermal field (13° 30.87´ N, 44° 59.24´ W) is situated near the base of the seamount, at a depth of 2570–2620 m (Fig. 2). It consists of a single mound or, probably, a series of coalesced sulfide mounds and their eroded products, each covered by metalliferous sediments and hydrothermal crusts (unpublished report of PMGE, 2007; Beltenev et al. 2007, 2009; Ivanov et al. 2008). The max size of the sulfide mound seen on the seafloor is ~175 × 200 m. The samples dredged in 2007 included serpentinized ultramafic rocks, altered basalts, and massive sulfides containing up to 20 volume percent of barite (Beltenev et al. 2007). Beltenev et al. (2009) also reported dredging small amounts of inactive chalcopyrite-rich chimneys. Recently, Melekestseva et al. (2014) reviewed the mineralogy, geochemistry, fluid inclusions data, and sulfur isotopic compositions of minerals hosted by colloform and fine-grained, barite-rich massive sulfides from the Semenov-1 hydrothermal field. It was shown that the Semenov-1 barite-rich marcasite–pyrite assemblages were formed from low-salinity fluids produced by phase separation of a Ba-rich hydrothermal fluid. Thermodynamic modeling showed that the formation of the Semenov-1 Ba-rich massive sulfides requires both a mafic substrate and a magmatic volatile contribution to the parent fluid.

The Semenov-3 hydrothermal field (13° 30.70´ N, 44° 55.00´ W) is located on the northeastern slope of the seamount at depths between 2400 and 2600 m, and is associated with altered basalts (Fig. 2). Sulfide breccia containing marcasite–pyrite clasts enclosed by sulfide–quartz cement, with numerous fractures and cavities encrusted with barite crystals, were also recovered from the seafloor in 2007, while massive sulfides dominated by pyrite and marcasite were dredged in 2009 (Beltenev et al. 2007, 2009).

Analytical methods

Barite-bearing samples from the Saf'yanovka deposit were collected from the main ore body in 2007–2010 from the open pit that was operating at the time. Massive sulfides from the Semenov-1 and -3 hydrothermal fields were collected using dredge station 30L186 and TV-grab station 30L292 (hereafter referred to as st. 186 and st. 292, respectively) from the Semenov-1 field and dredge station 30L284 (hereafter, st. 284) from the Semenov-3 field, respectively, during the 2007 cruise of the R/V *Professor Logachev* (Table 1).

Ten hand samples from the Saf'yanovka deposit and nine from the Semenov-3 field were studied macroscopically during this study. In addition, forty polished sections from Saf'yanovka and twenty from Semenov-3 were studied by transmitted and reflected light microscopy at the Institute of Mineralogy (IMin UB RAS), Miass, Russia. Major element compositions of barite from the Saf'yanovka deposit was analyzed at the IMin UB RAS using a REMMA-202M electron microscope equipped with a Link ED-System with a 1 μm electron beam, a 15 nA beam current, a 20 kV accelerating voltage and a counting time of 120 s for peaks; the standard used was MINM-25-53 from ASTIMEX Scientific Limited (mineral mount no. 01-044). Similarly, major elements for barite from the Semenov-3 fields were determined at IGG-CNR, Padova, Italy, using a CAMECA "CAMEBAX" SX-50 electron microprobe equipped with four vertical WDS spectrometers, a 1 μm electron beam, a 15 nA beam current, 15 kV accelerating voltage, and a counting time of 10 s for peaks and 10 s for background; the analytical standards were pure barite for Ba and S, celestite for Sr, wollastonite for Ca, sphalerite for Zn and galena for Pb. The contents of several minor and trace elements in selected barite samples were measured on an ELAN 9000 (PerkinElmer) quadrupole mass-spectrometer at the Zavaritsky Institute of Geology and Geochemistry (IGG UB RAS), Yekaterinburg, Russia, calibrated against the USGS rock standard BCR-2, using In as an internal standard.

Sulfur isotopic compositions of barite from the Saf'yanovka deposit and Semenov-3 hydrothermal field (reported as $\delta^{34}S$ per mil relative to the international standard CDT) were analyzed using a DELTA Plus XL, Thermo Finnigan mass-spectrometer using an NBS-127 standard at the Center of Analytical Researches, Karpinsky All-Russian Geological Institute (VSEGEI), St. Petersburg, Russia, and a Delta+ Advantage, Thermo Finningan mass-spectrometer using NBS-123 and IAEA-S-1 standards at IMin UB RAS.

Primary fluid inclusions (cf. Roedder 1984) were studied using double-polished sections using a THMSG-600 (LINKAM) equipment at the Laboratory of Thermobarogeochemistry, Faculty of Geology, South-Urals State University, Miass Branch, Russia. Homogenization, eutectic, and final ice melting temperatures were measured. Freezing experiments were always made first. For the Saf'yanovka deposit, which is associated with black shales, a pressure correction of +10 °C (Potter 1977) was made, based on the estimated pressure of formation of the deposit of 100–150 bar (Maslennikov 2006), which corresponds to the depth of deposition of modern black-shale sediments in the Red Sea and Black Sea (i.e., 1400 ± 500 m; Murdmaa 1987). For the Semenov-1 and Semenov-3 fields, a pressure correction of +25 °C was made, assuming a pressure of ~250–260 bars, which corresponds to a hydrostatic pressure regime under a water column of 2570–2620 m for the Semenov-1 and 2400–2600 m for the Semenov-3 fields (Beltenev et al. 2007). The salt compositions of the fluids were estimated after Borisenko (1977), who provided eutectic temperatures for 38 aqueous salt systems and combined them into five major groups: (i) LiCl-bearing (–74.8 to –78 °C); (ii) $CaCl_2$-bearing (–49.8 to –55 °C); (iii) $MgCl_2$-, $FeCl_2$-, and $FeCl_3$-bearing (–35 to –38 °C); (iv) NaCl- and KCl-bearing (–21.2 to –23.5 °C); and (v) sulfate- and carbonate-bearing (–1.2 to –6 °C). The salinities of the fluids were calculated from the temperatures of final ice melting following the methods of Bodnar and Vityk (1994).

Fluid inclusions in pure barite crystals from the Saf'yanovka deposit and the Semenov-3 field were further analyzed by pyrolisis–gas chromatography, which involves gas extraction from 50–150 mg samples by heating to 500 °C in a microfurnace. The compositions of the extracted gases were determined using a Tsvet-100 gas chromatograph equipped with a P-75 pyrolytic device at the Vernadsky Institute of Geochemistry and Analytical Chemistry, Russian Academy of Sciences

(GEOKHI RAS, Moscow) following (Mironova et al. 1992), The gases were accumulated in a precolumn at liquid nitrogen temperature and, then, rapidly introduced into a chromatographic column. Gases were determined using (i) a thermal conductivity detector (katharometer) for the registration of inorganic gases and water and (ii) a flame ionization detector for the registration of hydrocarbon gases. The duration of decrepitation was 3 min that is sufficient for the opening of inclusions in the samples but too short for the occurrence of secondary gas-forming reactions. The sensitivity of gas component determination was the following (μl): N_2 – 0.1, CH_4 – 4×10^{-2}, CO_2 – 3×10^{-2}, H_2O – 5×10^{-5}.

Ore microscopy

Barite was found in both colloform (Saf'yanovka, Semenov-1) and clastic (Saf'yanovka, Semenov-3) sulfide ores. The microstructural and paragenetic features of the barite-bearing ores are described here in detail.

Colloform sulfides

Saf'yanovka deposit

Samples from the upper part of the main sulfide body are characterized by colloform, zonal, and porous structures (Fig. 3a). In this sector, the hydrothermal precipitates are dominantly composed of pyrite and marcasite, with abundant quartz and barite, and minor chalcopyrite, sphalerite, tennantite, and galena. Barite forms tabular crystals up to 0.2 mm long and fills cavities in the sulfide matrix (Fig. 4a). It is associated with early quartz crystals up to 0.5 mm long and is cut by later, small-crystalline quartz. Locally, barite hosts small (10–20 μm) inclusions of pyrite and sphalerite. Crystalline aggregates of pyrite contain relics of an earlier, fine-grained, laminar, nodular and globular pyrite. The nodular pyrite is characterized by an outer rim of zonal crystalline pyrite.

Marcasite occurs as spear to tabular crystals and their aggregates, which are intergrown with crystalline pyrite. Rare small inclusions (up to 10 µm) of chalcopyrite, sphalerite, tennantite, and galena occur in pyrite.

Semenov-1 field

The main mineralogical and petrographical characteristics of the Semenov-1 hydrothermal field were described previously by Melekestseva et al. (2014). They are briefly summarized here and further integrated with additional specific details on barite. The massive sulfides are represented by porous, finely crystalline (st. 186), and colloform, nodular, porous, crystalline and banded (st. 292) marcasite–pyrite aggregates that contain barite and opal (Fig. 3b). At both sites, barite is the major gangue mineral, reaching up to 20 volume percent in single specimens from st. 186, and ~5 to 7 volume percent in those obtained from st. 292 (Melekestseva et al. 2014). Tabular barite crystals form elongated aggregates up to several mm long and ~1 mm thick, or pockets made up of rosettes ~1.5 mm across (Fig. 4b). Barite crystals are characterized by growth zoning, which is marked by pores and an abundance of fluid inclusions. Early and late generations of barite can be distinguished. For example, early, relatively large (up to 1 mm) barite crystals are in part pseudomorphically replaced by sulfides and are themselves mantled by sulfides. Later, much smaller (~50 µm) barite crystals overgrow the late-generation sulfides.

At st. 186, a fine-crystalline (~10 µm) pyrite is associated with quartz and is overgrown by a coarse-crystalline pyrite. At st. 292, tiny (~1 µm) pyrite globules, clustered into framboids (up to 20 µm), are partially replaced by pyrite crystals (up to 20 µm). Marcasite occurs as two generations of spear and tabular crystals (10 µm–1 mm), which are overgrown by a crystalline pyrite. Numerous small (up to 40 µm) sphalerite grains and occasional inclusions of galena were observed in both pyrite and barite. Fine inclusions of chalcopyrite (1–2 µm) and pyrrhotite (up to 8 µm) were observed in crystalline pyrite as small inclusions. Chalcopyrite is also intergrown with sphalerite, or forms “chalcopyrite disease” in sphalerite. Isocubanite was rarely found as isometric inclusions (up to 50 µm) in sphalerite. Sulfides and barite from st. 186 are coated by a thin (~20 to 50 µm) rim of opal. Hematite forms numerous clots in the late opal, or occasional globules on the sulfides. Late Fe-hydroxides and jarosite pseudomorphically replace the sulfides.

Clastic ores

Saf'yanovka deposit

The margins of the main Saf'yanovka ore body are host to numerous clastic ores (e.g., Safina and Maslennikov 2009). On its southern flank, sulfide breccias are found which are cemented by barite, quartz and, locally, by carbonaceous silty sandstones (Fig. 3c). The breccias are mainly composed of pyrite and marcasite with lesser sphalerite, galena, quartz, and barite and sporadic chalcopyrite and tennantite.

Barite occurs in the cement as compact aggregates of deformed, broken, or slightly curved tabular crystals up to 1 mm in size (Fig. 4c) or as relict crystals in clasts of colloform pyrite ores. Small (~10 µm) pyrite crystals, intimately intergrown aggregates of sphalerite and galena, and rare grains of chalcopyrite and tennantite are locally observed in barite crystals. Chains of finely crystalline quartz are observed between individual plates of barite, or within them. Angular pyrite clasts up to 3 cm in size are characterized by colloform, framboidal, crystalline, granular, laminar, nodular and/or globular structures. Clasts of laminar and nodular pyrite are interpreted to represent fragments of seafloor hydrothermal crusts, fossilized fauna from the outer-zone of mineralized material, and black smoker chimneys. Clasts of framboidal pyrite are cemented by fine-grained anhedral pyrite, marcasite or gangue minerals, and served as a core for the late pyrite aggregates. Some clasts, where pyrite replaces pyrrhotite, contain individual or clustered, elongated, oval and round pseudomorphs after near-hydrothermal fauna, set in a fine-grained clastic sulfide matrix. Clasts of radial aggregates and occasional dendrites of marcasite are common. Relics of colloform pyrite are locally found in fine-grained marcasite. Sphalerite, galena, tennantite, and chalcopyrite are observed as small (3–5 μm) inclusions in the pyrite clasts.

Semenov-3 field

Sulfide breccias are composed of angular clasts of colloform, concentric-zonal, massive, and porous marcasite–pyrite aggregates up to 10 cm across that are cemented by fine-grained clastic sulfides and quartz (Fig. 3d). Pyrite, marcasite, and quartz are the dominant minerals, and are accompanied by lesser amounts of barite, chalcopyrite, hematite, and jarosite, and occasional bornite, sphalerite, pyrrhotite, and covellite.

Tabular barite crystals up to 1 mm in size fill numerous fractures and cavities in the marcasite–pyrite clasts and cement and form druses or rosettes up to 0.5 cm thick (Fig. 4d). They are locally associated with late chalcopyrite. Quartz forms the cement of the breccias and overgrows the pyrite clasts and barite crystals. Colloform and nodular pyrite clasts consist of porous dendritic early pyrite and zonal crystals of later pyrite. Marcasite occurs as radial aggregates up to 1 mm in size made of spear crystals or of intergrown, zonal crystals with rhombic sections. Pyrite and marcasite are also closely associated with concentric-zonal aggregates. Chalcopyrite is found as individual round grains, anhedral aggregates, and occasional euhedral crystals in the cement and fractures and pores of the marcasite–pyrite aggregates locally associating with barite. Bornite forms small (~10 μm) grains surrounded by chalcopyrite in the cement or in the late quartz rims. Micron-sized covellite rims are developed around the chalcopyrite grains. Small (up to 10 μm) subhedral sphalerite and pyrrhotite grains occur in the pyrite clasts. Hematite is found as globules in the quartz rims around pyrite or as acicular crystals in cement. Jarosite zones up to 50 μm thick are developed in the marginal and central portions of marcasite–pyrite clasts.

Chemical composition of barite

Strontium is the most abundant minor component in barite based on microprobe and ICP-MS analyses (Tables 2 and 3). Barite from the Saf'yanovka deposit contains less SrO (up to 1.05 wt% in microprobe analyses and 2530 to 3100 ppm Sr in ICP-MS analyses) than that from the Semenov-1 (up to 4.12 wt% SrO and 7050 ppm Sr; Melekestseva et al., 2014) or Semenov-3 (up to 3.36 wt% SrO and 3410 ppm Sr) hydrothermal fields. However, in general, there is no univocal relationship between SrO contents in barite and the various ore facies.

Barite from Semenov-1 field contains minor to trace PbO (0.02–0.16 wt%), CaO (0.01–0.38 wt%), ZnO (0.01–0.05 wt%) and FeO (0.12–0.40 wt%). Semenov-3 barite is zoned, with higher SrO (up to 4.73 wt%) and PbO (up to 0.5 wt%) contents in the core, and lower contents (0.24–1.06 wt% and < 0.1 wt%, respectively) in the margins. Barite from the Saf'yanovka colloform ores contains only minor admixtures of CaO (0.03–0.11 wt%), which was not detected in barite derived from the clastic ores.

At Saf'yanovka, barite from the clastic ores is enriched in several trace elements (i.e., Cu, Zn, Pb, Ga, As, Hg, Bi, Mn, and Sr) when compared with barite from the colloform ores (Table 3). Barite from the colloform ores has relatively increased contents of nickel only (i.e., 15.1 vs 6.6 ppm). The contents of Ge, Se, Cd, Tl, Sb, Te, Co, Y, and V are relatively low (and similar) in both varieties of barite.

Similarly, barite from the Semenov-3 breccias is enriched in many trace elements (Cu, Pb, Ga, Ge, Cd, Sb, Co, Ni, and V) relative to barite from the Semenov-1 finely crystalline sulfides. However, barite from the Semenov-3 clastic sulfides has lower contents of Zn, Mn, and Sr. Other trace elements (i.e., As, Se, Te, Tl, Bi, and Y) show no significant variations between the two varieties of barite.

Sulfur isotopic composition of barite

The sulfur isotopic compositions of the analyzed barites vary within a single deposit, or cluster (Table 4). The $\delta^{34}S$ values of barite from the Saf'yanovka colloform ores show a relatively wide range (from +20.9 to +25.5‰), whereas the $\delta^{34}S$ values of barite from the Saf'yanovka clastic ores are higher and show a narrower range (from +27.0 to +29.2‰). The $\delta^{34}S$ values of barite from the Semenov-1 colloform sulfides (from +21.0 to +21.3‰; Melekestseva et al. 2014) are higher than those of barite from the Semenov-3 clastic sulfides (from +18.7 to +20.6‰).

Fluid inclusion data

Fluid inclusions in barite from the Saf'yanovka colloform ores are 10 to 40 μm in size and are characterized by negative-crystal to subround shapes. The negative-crystal inclusions are mostly one-phase (liquid), whereas subround inclusions are vapor-rich and two-phase (liquid + vapor). In the liquid two-phase inclusions the vapor bubbles occupy 20–30 volume percent of the inclusions. In the vapor-rich inclusions the relative proportion of liquid and vapor was difficult to assess. Similar fluid inclusions ranging 5 to 30 μm in size are unevenly distributed in barite from the Saf'yanovka clastic ores.

Rare angular, round, or spindle-like fluid inclusions (8–12 μm, occasionally up to 20 μm long) are uniformly distributed in barite within the Semenov-1 field (Melekestseva et al. 2014). The majority of them are two-phase fluid inclusions composed of liquid and a vapor bubble, which occupies 5–10 vol.% of the inclusions. More rare, small groups of two-phase inclusions, partly showing negative crystal shapes, consist of liquid and a larger vapor bubble, which occupies up to over 50 vol% of the inclusion. At the Semenov-3 field, negative-crystal or elongated fluid inclusions <10 μm in size are unevenly distributed in barite. Both one- (liquid) and two-phase (liquid + vapor) inclusions, with a vapor bubble occupying 15–20 volume percent of the inclusion are found.

The results of heating and cooling measurements on liquid-rich, two-phase inclusions are summarized in Table 5. Upon heating, the inclusions in barite from colloform sulfides homogenize to the liquid phase at 162 °C to 184 °C (average and median 173 °C, mode 177 °C) in the Saf'yanovka samples, and at 58 °C to 199 °C (average, median and mode at 150 °C) at the Semenov-1 samples (Fig. 5a, c). The homogenization temperatures of fluid inclusions in barite from clastic sulfides range from 130 °C to 170 °C (with two modes at 135–140 °C and 155–160 °C, average at 150 °C, and median at 149 °C) in the Saf'yanovka samples and from 241 °C to 310 °C (average, median and mode at 275 °C) in the Semenov-3 samples (Fig. 5e,g). Effects of possible stretching of fluid inclusions were minimized by studying mostly small-sized, round inclusions, as suggested by Ulrich and Bodnar (1988). The relatively narrow ranges of homogenization temperatures and absence of high-*T* outliers within each sample population (Fig. 5a), as well as the lack of correlation between homogenization temperatures and inclusion size further suggest that stretching was effectively minimized. The above data should therefore be reliable.

Final temperatures of ice melting are –0.9 to –2.7 °C (Saf'yanovka colloform ores), –0.5 to –2.8 °C (Semenov-1 colloform sulfides), –0.8 to –3.3 °C (Saf'yanovka clastic ores), and –3.0 to –6.0 °C (Semenov-3 clastic sulfides). According to Bodnar and Vityk (1994), these values correspond to salinities of 1.6 to 4.5 wt% $NaCl_{eq}$ (average, median and mode of 2.9 wt%), of 0.6 to 3.8 wt% NaCl equivalent (average, median and mode of 2 wt%), 1.4 to 5.4 wt% $NaCl_{eq}$ (average of 3.9 wt%, median of 4.2, and two modes at 2.5–3.0 wt% and 4.5–5.0 wt%), and 4.8–9.2 wt% $NaCl_{eq}$ (average, median and mode of 6.7 wt%; Figs. 5b, d, f, h), respectively. The temperature vs. salinity dependence is either absent (Saf'yanovka and Semenov-3) or weakly positive (Semenov-1 barite) (Fig. 6).

The eutectic temperatures of fluid inclusion in barite from the Saf'yanovka and Semenov-1 colloform sulfides vary from –21.7 to –22.3 °C and from –2.2 to –6.6 °C, respectively. These values are compatible with a $NaCl–Na_2CO_3–H_2O$ system, with possible addition of Na_2SO_4 and $NaHCO_3$ for the Saf'yanovka deposit and with $Na_2SO_4–K_2SO_4–H_2O$ and $Na_2SO_4–NaHCO_3–H_2O$ systems for the Semenov-1 field (cf. Borisenko 1977; see also Melekestseva et al. 2014). The eutectic temperatures of fluid inclusions in barite from the clastic ores range from –22.0 to –22.3 °C in the Saf'yanovka deposit and from –21.1 to –21.8 °C in the Semenov-3 field. These values are compatible with a NaCl-dominated composition, with possible addition of Na_2SO_4 and $NaHCO_3$ for the Saf'yanovka breccias (cf. Borisenko 1977).

Gas chromatography data (Table 6) show that the fluid inclusions, as expected, are dominated by H_2O. Inclusions in barite from the Saf'yanovka colloform ores are enriched in CH_4, CO_2, and CO relative to those from the Saf'yanovka clastic ores. Inclusions in barite from the Semenov-3 clastic ores have higher contents of CO_2 than those from the Saf'yanovka clastic ores and have the highest CO_2/CH_4 ratios. Other potential volatile components, such as H_2S, SO_2 or various hydrocarbons, which are typical of hydrothermal vents (e.g. Gieskes et al. 1988; de Ronde et al. 2003, 2011), were below detection limits in all analyzed samples. These data can be compared with those of Krylova and Melekestseva (2011), who qualitatively estimated by Raman spectroscopy the composition of vapor in fluid inclusions in barite from Semenov-1 st. 186: spectra in the range 1100–2000 cm^{-1} showed peaks at 1150 cm^{-1}, compatible with the presence of SO_2, and at 1370 and 1388 cm^{-1}, indicating the presence of CO_2 (cf., Naumov et al. 1986; Frezzotti et al. 2012).

Discussion

Barite is a common gangue mineral in ancient VMS deposits of the Kuroko type associated with felsic rocks (cf. Sato 1977; Scott 1980; Ohmoto 1996) and in modern arc-related and sediment-hosted hydrothermal fields (cf., Gieskes et al. 1988; Hannington and Scott 1988; Shadlun et al. 1992; Binns and Scott 1993; Fouquet et al. 1993a; Goodfellow and Franklin 1993; Halbach et al. 1993; Herzig et al. 1993; Zierenberg et al. 1993; Davis et al. 2003; de Ronde et al. 2003, 2005; Glasby et al. 2008; Berkenbosch et al. 2012; Hein et al. 2014). Barite is instead rare in most mafic-hosted hydrothermal fields on slow-spreading ridges (Fouquet et al. 1993b; Rona et al. 1993;

Duckworth et al. 1995; Halbach et al. 1998) and in their ancient, Cyprus-type VMS analogs (cf. Constantinou and Govett 1972; Ixer et al. 1984; Hannington et al. 1998). The abundance of barite in the Semenov-1 and -3 hydrothermal fields, as well as in the Lucky Strike, Menes Gwen, and Krasnov hydrothermal fields of the MAR (Fouquet et al. 1994; Bogdanov et al. 2006; Cherkashev et al. 2008), is thus somewhat anomalous. The Fe-disulfide-rich and barite-rich composition of the colloform and clastic ores of the backarc-hosted Saf'yanovka VMS deposit is similar to that of the Semenov-1 and -3 hydrothermal fields, which suggests similar formation condition, in spite of different geodynamic setting. The significance of such similarities is discussed below.

Textural-structural and mineralogical features

The abundance of finely crystalline, porous, nodular, banded, and colloform structures, the predominance of pyrite and marcasite, and the presence of barite with less abundant SiO_2 phases in *colloform* sulfides from both the Saf'yanovka deposit and Semenov-1 hydrothermal field suggest formation under comparable physico-chemical conditions. The morphological features of barite crystals and aggregates in colloform sulfides from both deposits are typical of hydrothermal barites (cf. Paytan et al. 2002; de Ronde et al. 2005; Berkenbosch et al. 2012). The abundance of pyrite and marcasite points to the predominance of Fe over chalcophile metals and relatively high sulfur activity (Hannington and Scott 1989). Despite the strict association of barite and sulfides, precipitation of barite in colloform sulfides from the Saf'yanovka deposits and Semenov-1 field appears to postdate and predate, respectively, that of the accompanying sulfides, therefore it remains unclear whether barite and sulfides could have been part of the same paragenesis. Similar low- to medium-temperature massive sulfides with simple mineral compositions and dominant pyrite and marcasite are well documented at the flanks of seafloor sulfide mounds (e.g., TAG and Snake Pit hydrothermal fields, Mid-Atlantic Ridge; Fouquet et al. 1993; Rona et al. 1993). Barite chimneys with pyrite were reported on the flanks of the Loki's Castle and Jan Mayen hydrothermal fields in the Arctic mid-Oceanic Ridge (Eickmann et al. 2010; Pedersen et al. 2010). These conditions appear to be distinct from those of seafloor, barite-rich assemblages recovered from arc-related hydrothermal systems, where barite is mostly associated with Cu-rich or polymetallic sulfides: e.g., Cu-rich and Zn-rich chimneys at the Brother volcano (de Ronde et al. 2003), Cu-rich chimneys in the PACMANUS hydrothermal field (Binns and Scott 1993) or sphalerite-dominated chimneys in hydrothermal fields of the Lau basin (Herzig et al. 1993). At the same time, the pyrite-rich samples recovered from the Brother volcano showed the presence of anhydrite instead of barite (de Ronde et al. 2005). The Fe-rich sulfides with barite from the White Lady hydrothermal field in the North Fiji basin represent spires rather than colloform massive sulfides (Bendel et al. 1993). The Fe-rich assemblage with barite from the JADE hydrothermal field in the Okinawa Trough replaces primary Cu– and Zn–rich assemblages (Halbach et al. 1993).

Clastic ores from the Saf'yanovka deposit resemble those from the Semenov-3 hydrothermal field in several respects. That is, the combination of sulfide clasts with colloform, finely crystalline, banded, and massive textures, the significant proportions of sulfide–quartz cement, the presence of host-rock clasts, the mineral composition (i.e., major and accessory sulfides), and the abundance of barite and quartz. Barite in breccias from both deposits was formed after the cementation of the breccia. Barite from the Saf'yanovka clastic ores precipitated after formation of diagenetic pyrite framboids and metacrystals, and its compact aggregates are similar to those of diagenetic barite from oceanic sediments (Paytan et al. 2002). The barite crystals are deformed and locally show stylolite boundaries as a result of burial and compaction (Fig. 4c). Therefore, its origin can be defined as 'anadiagenetic' (cf. Fairbridge 1967). In contrast to Saf'yanovka deposit, barite in clastic sulfides from the Semenov-3 field is most probably a product of mixing of late hydrothermal fluid with seawater. It occurs in large cavities in clasts and cement, forms radial aggregates of large tabular crystals, which are typical of active hydrothermal chimneys (e.g., Fouquet et al. 1993a; de Ronde et al. 2003), is locally associated with late chalcopyrite with high Se content (638–1201 ppm, unpublished LA-ICP-MS analysis by I.Yu. Melekestseva). The high Se contents in chalcopyrite are considered as evidence of high-temperature and highly reducing conditions (Maslennikov et al. 2009). A late hydrothermal origin is consistent with ^{230}Th/U dating of massive sulfides from station 30L284, which showed multi-stage hydrothermal activity at the Semenov-3 hydrothermal field with at least four peaks at ~90, 51, 47, and 35 ka (Kuznetsov et al. 2011).

Formation conditions of barite

Pressure-corrected homogenization temperatures of fluid inclusions in barite from the barite-rich *colloform* sulfides are 172–194 °C for the Saf’yanovka deposit and 83–224 °C for the Semenov-1 field (Table 5). The widespread presence of marcasite, which forms at temperatures <240 °C (Murowchick and Barnes 1986), is consistent with formation of the colloform sulfide–barite association at moderate to low temperatures. Assuming isotopic equilibrium was attained, the δ^{34}S fractionation between barite and colloform sulfides at Semenov-1 would yield a temperature of 239 °C. This estimate is consistent with fluid inclusions data if uncertainties of sulfur isotope thermometry are taken into account (±10 to ±40 °C; cf. Seal 2006). The same calculation for the Saf’yanovka samples yielded a temperature of 265 °C, which clearly indicates isotopic disequilibrium, consistent with the interpreted late origin of barite relative to the colloform sulfides. The formation temperatures estimated for the colloform sulfides–barite associations (172–225 °C) are consistent with the typical formation conditions of seafloor white smokers, in which barite is predominant over other gangue minerals (<300 °C; Hannington et al. 1995).

The pressure-corrected homogenization temperatures of fluid inclusions in barite in the Saf’yanovka *clastic* ores (140–180 °C), which we interpret to be anadiagenetic based on microtextural features (see above), are within the range of diagenetic processes (up to 200 °C; e.g., Yapaskurt 2005). The higher homogenization temperatures of fluid inclusions in barite from the Semenov-3 clastic sulfides (266–335 °C) reflect its formation from a relatively high-temperature hydrothermal fluid, which is also supported by its association with late Se-rich chalcopyrite (see above).

The relationship between barite formation temperatures and mineralogy of associated sulfides is in line with estimates from other modern seafloor hydrothermal sites. In general, pure barite precipitated on chimney rims or found as massive fragments records relatively low temperatures (ca. 150–200 °C), barite associated with sphalerite and polymetallic sulfides records moderately high temperatures (214–280 °C), and barite associated with chalcopyrite–pyrite records the highest temperatures (up to at least 290 °C) (Herzig et al. 1993; Petersen et al. 2004; de Ronde et al. 2003).

Chemical composition of barite

Strontium is one of the most abundant minor components in barite (Deer et al. 1962; Hanor 2000). The barites studied have low SrO contents (0.00–4.73 wt%), especially those from the Saf'yanovka deposit (up to 1.05 wt%). Reported SrO contents in different genetic types of barite, including examples from ancient massive sulfide deposits and modern hydrothermal sulfide fields, are highly variable. For example, both ancient and modern seafloor hydrothermal barites typically contain small amounts of SrO (e.g., 0.6–3.5 wt% SrO, Franklin Seamount, Woodlark basin, Binns et al. 1993; 0.07–0.22 wt% SrO, Devonian Balta-Tau VMS deposit, South Urals, Holland 2002; average 0.50 wt% SrO, Mesoproterozoic stratiform Pb-Zn-Cu±Au-Ba deposits, South Africa, McClung et al. 2007). Modern seafloor specimens rarely exceed 10 wt% of SrO (e.g., up to 11.85 wt% SrO, barite–sulfide edifice, Loihi Seamount, Hawaii, Davis et al. 2003; up to 11.9 wt% SrO, barite chimneys, Gulf of Mexico, Fu et al. 1994). Low to intermediate SrO contents are reported in marine biotic barite (e.g., <0.05 wt% SrO, central North Pacific seafloor; Bertram and Cowen 1997) and in cold-seep barite (1.05–5.45 wt% SrO, shallow hemipelagic sediments with sulfides, Middle Valley field, Juan de Fuca Ridge, Goodfellow and Blaise 1988; up to 4 wt% SrO, Deryugin Basin, Sea of Okhotsk, Greinert et al. 2002; 0.15–1.52 wt% SrO, San-Andreas fracture zone, Pacific Ocean; Hein et al. 2007). Overall, the range of SrO contents in barite appears to be irrespective of its origin, suggesting that the degree of strontium enrichment may either be related to fluctuation of Sr contents in the parent fluid or reflect variable mixing of these fluids with seawater. Mixing with Sr-rich seawater may account for variable Sr contents in Saf'yanovka (and perhaps Semenov) hydrothermal barite, because barite from deeper, stockwork pyrite–sphalerite ores contain less Sr (up to 944 ppm) (Murzin et al. 2010). Higher Sr levels in diagenetic barite from the Saf'yanovka clastic ores may indicate contribution from connate seawater and from alteration of clasts of plagioclase-rich host rocks.

The measured contents of Cu and Zn (Pb) in barite from the Saf'yanovka *colloform* ores and the higher contents of Zn in barite from the Semenov-1 field are probably related to micro-inclusions of sulfides (e.g., sphalerite, chalcopyrite and galena), which were recognized during the petrographic study. The higher Sn contents in barite from the Semenov-1 field may also be attributed to sphalerite inclusions, since sphalerite may contain Sn as trace element (Cook et al. 2009). The relatively high contents of Ni (and Co) found in Semenov-1 barite are not unusual for seafloor hydrothermal barite (cf. Davis et al. 2003; Ludwig et al. 2006). These high contents may derive from seawater, as significant sorption of these elements occurs on barite after a long period of interaction with seawater (Jewell and Stallard 1991). A similar process was proposed for Ni-enriched barite from inactive carbonate edifices at the Lost City low-temperature ultramafic-associated field (Ludwig et al. 2006). Incorporation of Co and Ni from seawater rather than from the parent fluid is supported by the trace element compositions of associated pyrite and marcasite, which are both Co- and Ni-free (Melekestseva et al. 2014). The higher Mn contents in barite from the Semenov-1 field relative to other studied barites may also have derived from seawater.

Barites from the Saf'yanovka and Semenov-3 *clastic* ores are enriched in several trace elements when compared to barite from the colloform sulfides. In particular, the enrichment of Semenov-3 chalcopyrite-associated barite in several chalcophile elements (e.g., Cu and, to a lesser extent, Ga, Ge and Sb) is probably a real feature, since no micro-inclusions of chalcopyrite were observed in such barite. By contrast, the relatively high contents of Co (44 ppm) and Ni (437 ppm) probably reflect the presence of inclusions of clastic crystalline pyrite, which contain high Co (266–1444 ppm) and Ni contents (216–127 ppm Ni; I. Melekestseva, unpublished data). The higher Zn, Pb, As, Te, Hg, and Bi contents in barite from the Saf'yanovka clastic ores are probably due to micro-inclusions of sphalerite, tennantite, and galena observed during the petrographic studies.

Sources of sulfur

The average $\delta^{34}S$ value for barite from *colloform* ores of the Saf'yanovka deposit (+22.9‰) corresponds to that of Silurian–Devonian seawater (+23 to +24‰, Claypool et al. 1980). The average $\delta^{34}S$ value for barite from colloform sulfides of the Semenov-1 field (+21.2‰; Melekestseva et al., 2014) matches the composition of contemporary seawater (+21.2‰, Rees et al. 1978). These results clearly indicate a seawater source for SO_4^{2-} for both hydrothermal barites.

The average $\delta^{34}S$ values for barite from *clastic* ores of the Saf'yanovka deposit (+28.1‰) are significantly higher than that of Silurian–Devonian seawater (+23 to +24‰, Claypool et al. 1980), which may indicate partial reduction of seawater sulfate and concurrent isotopic enrichment of the residual sulfate (Shanks et al. 1995). Sulfate sulfur may be reduced by bacterial or thermochemical reduction (Machel 2001). Bacterial sulfate reduction, which is typically invoked for diagenetic barites (Paytan et al. 2002; Hein et al. 2007), is believed to occur from 0 °C to about 60–80 °C (Machel 2001). Thermochemical sulfate reduction is common at temperatures of 100–180 °C (Machel 2001) and may arise from interaction with ferrous minerals and/or organic matter in the shallower parts of hydrothermal system (Shanks et al. 1995; de Ronde et al. 2003). The pressure-corrected homogenization temperatures of fluid inclusions in barite from clastic ores of the Saf'yanovka deposit (140–180 °C) support thermochemical rather than biological sulfate reduction.

All measured $\delta^{34}S$ values of barite from the Semenov-3 field (average = +19.6‰) are lower than that of seawater, which suggests partial sulfate contribution from the oxidation of isotopically lighter H_2S in vent fluid or sulfide minerals (Shanks et al. 1995). This is in agreement with the association of barite with late-stage chalcopyrite, which is believed to have precipitated from a relatively reduced, H_2S-bearing fluid (see above). Similar $\delta^{34}S$ values lower than seawater were reported in barite from the Axial Seamount, Juan de Fuca Ridge (+16.1 to +21.2‰; Hannington and Scott 1988) and Franklin Seamount, Woodlark Basin (+19.2 to +20.9‰; Binns et al. 1997).

Fluid compositions

Salinities of liquid-rich fluid inclusions in hydrothermal barite from Saf'yanovka and Semenov-1 colloform sulfides are mostly lower than seawater (3.2 wt% NaCl equiv.; Bischoff and Rosenbauer 1984; see Fig. 6) and among the lowest reported for massive sulfide deposits and seafloor hydrothermal fields (e.g., Lecuyer et al. 1999; Dahlmann et al. 2001; de Ronde et al. 2003; Petersen et al. 2004; Bortnikov et al. 2004; Scotney et al. 2005; Simonov et al. 2006). The coexistence with vapor-rich inclusions suggests that the fluid was boiling during barite formation, so that the original fluid could have been even less saline. Following a widely accepted view (e.g., Cowann and Cann 1988; Massoth et al. 1989; Butterfield et al. 1990; Bortnikov et al. 1997; de Ronde et al. 2003; von Damm et al. 1998; 2003; Petersen et al. 2004; Suzuki et al. 2006), Melekestseva et al. (2014) interpreted the low salinity of fluid inclusions in Semenov-1 barite as being due to phase separation of an aqueous fluid below the seafloor and this conclusion may be extended to barite in Saf'yanovka colloform sulfides.

The calculated salinities of the fluid inclusions in late hydrothermal barite from the Semenov-3 breccia are 1.5 to 2.9 times that of seawater (Table 4). Relatively high salinities are typical of fluid inclusions in many hydrothermal sulfide fields. However, in most cases, the salinities show a range of values from near- or less-than-seawater values, to higher-than-seawater values (e.g., Binns et al. 1993; Herzig et al. 1993; Petersen et al. 2000; Lüders et al. 2001; Bogdanov et al. 2002; de Ronde et al. 2003; Bortnikov et al. 2004; 2005; Cazañas et al. 2008). This range is invariably explained by phase separation, followed by remixing of separated vapor and liquid phases during ascent, probably with some brine loss at depth (e.g., at the TAG field with salinities of 1.9 to 6.2 wt.% NaCl equiv.; Petersen et al. 2000). Such a variability of salinity values is not observed in our Semenov-3 samples. However, the high salinity values may still be a result of phase separation, if only the high-density brines were trapped or if they where expelled independently at a late stage (cf. Gruen et al. 2014). As an alternative, the high salinities may be related to a contribution of magmatic fluid (cf. Nehlig 1993; de Ronde et al. 2011). Taking into account the high CO_2 contents of the fluid inclusions (Table 6), a magmatic contribution is likely. The variable salinity of fluid inclusions in anadiagenetic barite from the Saf'yanovka clastic ores (1.4–5.4 wt% NaCl equiv.), for which a late hydrothermal origin is not supported (see above), probably reflects involvement of several sources of water: (i) connate seawater (Fairbridge 1967), (ii) high-salinity water from dehydration of layered silicates (cf. Kelly and Delaney 1987) and (iii) low-salinity water released from fluid inclusions in dissolved or mechanical deformed primary hydrothermal barite.

In general, volatiles in the fluid inclusions in the studied barite are dominated by H_2O followed by CO_2 with lesser amount of CO, CH_4, and N_2. The presence of CO_2 may be related to contribution from different sources (magma, seawater, interaction with organic matter or host rocks). In case of Saf'yanovka colloform ores with plentiful fauna relics, the high CO_2 contents may be provided by oxidation of CH_4 (according to reaction $CH_4 + 2\ O_2 = 2\ H_2O + CO_2$) or organic matter. The high contents of CO_2 in Semenov-3 barite are most likely due to magmatic contribution (cf. Butterfield et al. 1990; Lilley et al. 2003; de Ronde et al. 2003), consistent with the higher salinity of fluid inclusions. The presence of SO_2 (1150 cm^{-1}) and CO_2 (1370 and 1388 cm^{-1}) peaks in the Raman spectra of the fluid inclusions from Semenov-1 field (Krylova and Melekestseva, 2011) may also reflect magmatic contribution to the hydrothermal fluid similar to that observed at some high-temperature seafloor sulfide edifices such as Brothers volcano of the Kermadec arc (de Ronde et al. 2011) or NW Rota-1 volcano of the Mariana arc (Butterfield et al. 2011), or at other arc magmatic-hydrothermal sites such as Kasuga seamount also of the Mariana arc, or hot spot volcanoes such as McDonald seamount and Loihi seamount (McMurty et al. 1993). Based on thermodynamic modeling, a magmatic contribution has also been suggested as essential for the formation of Fe-disulfide–barite-rich association at Semenov-1 (Melekestseva et al. 2014).

The higher contents of CH_4 in fluid inclusions from the Saf'yanovka colloform ores may be related to decomposition of hydrothermal fauna or interaction with black shales (cf. Lilley et al. 1993, 2003; de Ronde et al. 2003). Although an abiogenic origin of CH_4 cannot be excluded (cf. Lilley et al. 1993), the abundant near-hydrothermal macro- and microfauna and the presence of associated black shales at the Saf'yanovka deposit support its biogenic genesis.

The source for N_2 in the Saf'yanovka barites is uncertain, because it may be derived from seawater (Lilley et al. 2003; Steele et al. 2010), from magmas (cf. de Ronde et al. 2003) or from oxidation of hydrothermal ammonium and its microbial assimilation (Lam et al. 2004; Lang et al. 2012). A derivation from oxidation of hydrothermal ammonium, which may be originated from the decomposition of subseafloor organic matter in sediments (Lilley et al. 1993), is a plausible hypothesis, given the presence of black shales and macro- and microfauna at the Saf'yanovka deposit. A magmatic source cannot be excluded, but it seems less likely, since no other magmatic indicators are found in the studied barite. The increase of one order of magnitude in the proportion of N_2 in barite from the Saf'yanovka clastic ores appears consistent with its diagenetic formation, as nitrogen may be generated during thermal decomposition of organic matter in clay-rich sedimentary rocks (cf. Littke et al. 1995; Hao et al. 2002).

Overall, the analyzed fluid inclusions in barite at Saf'yanovka and Semenov-1 and -3 have lower H_2O, significantly higher CO_2 and CH_4, and comparable N_2 contents relative to barite in massive sulfides from the Brothers volcano, Kermadec arc (de Ronde et al. 2003), or barites from the Myojinsho and Myojin Knoll vent sites, Izu-Bonin arc (Sasaki et al. 1995). This suggests that the parent fluids were either more volatile-rich or less diluted by seawater, similar to what proposed for the Myojinsho and Myojin Knoll vent sites (cf. de Ronde et al. 2003). The presence of CO in the studied fluid inclusions indicates that the hydrothermal fluids from the Saf'yanovka deposit and

Semenov-3 field were not fully oxidized in comparison with the above mentioned hydrothermal sites.

Conclusions

The comparative study of barite from colloform and clastic ores from the Paleozoic Saf'yanovka VMS deposit and modern inactive Semenov-1 and -3 hydrothermal fields indicates that morphology is the most distinctive feature in different types of barite. Hydrothermal barite in both ancient and modern colloform ores shows undeformed, tabular to platy morphology, with or without formation of rosette aggregates. This type of barite may locally be replaced by sulfides. In contrast, non-hydrothermal, diagenetic barite (observed in the Saf'yanovka clastic ores) occurs as compact aggregates of deformed, broken, or slightly curved platy or tabular crystals. Stylolite boundaries characteristically occur between the deformed crystals. Stylolites and deformation indicate development of pressure and strain during anadiagenetic crystallization within the buried clastic ores.

The chemical and sulfur isotopic compositions of barite and the compositions of fluid inclusions in it show a significant variability, but wide overlaps are observed between different genetic types. The variable contents of Sr, the main minor component in barite, essentially reflect variable contribution of this element from seawater (for both hydrothermal and non-hydrothermal barite) and, possibly, from plagioclase-rich host rocks (for non-hydrothermal barite). Apparent variations in several trace elements are mostly ascribed to contamination from sulfide micro-inclusions. The sulfur isotopic compositions of hydrothermal barite generally indicate seawater as the main source of sulfur, although additional contribution of isotopically light sulfur from partial oxidation of H_2S (Semenov-3 field, this study; Axial Seamount, Hannington and Scott 1988; Franklin Seamount, Binns et al. 1997; Hine Hina field, Herzig et al. 1998) or of isotopically heavy sulfur from bacterial sulfate reduction (Loki's Castle field, Eickmann et al. 2010) is also documented. A contribution from isotopically heavy sulfur remaining after partial reduction of seawater sulfate appears to be common in non-hydrothermal, diagenetic barite, although the mechanism of sulfur reduction may vary (i.e., thermochemical sulfate reduction for the Saf'yanovka deposit studied in this work vs. bacterial sulfate-reduction for diagenetic barite; cf. Paytan et al. 2002; Hein et al. 2007).

In spite of different geodynamic setting, barite-bearing pyrite-rich colloform ores from the Saf'yanovka VMS deposit (back-arc basin) and Semenov-1 and -3 hydrothermal fields (slow-spreading mid-oceanic ridge) were formed under similar, low- to moderate-temperature conditions (83–233 °C). Temperatures as high as 335 °C are estimated for some late-stage hydrothermal barites from Semenov-3 clastic sulfides, which are associated with Se-rich chalcopyrite. Diagenetic barite in Saf'yanovka clastic pyrite ores records moderate temperatures of 140–180 °C. Combining our new data with those for other seafloor hydrothermal barites the following systematics can be defined: barite precipitated on chimney rims or associated with pyrite-rich colloform sulfides forms at relatively low to moderate temperatures (ca. 80–230 °C); barite associated with sphalerite-rich and polymetallic massive sulfides forms at moderately high temperatures (210–280 °C), and barite associated with chalcopyrite records the highest temperatures (265–335 °C).

Acknowledgements

The authors thank I. Kislyuk, N. Ivanova, G. Lonshchakova, L. Udachina, D. Kiseleva, R. Carampin, T. Nazarova, O. Mironova and R. Sadykova for their help in sample preparation and analytical work. I.Yu.M is grateful to Victor Ivanov and Victor Beltenev (PMGE, St. Petersburg, Russia) for participation in the 30th cruise of *R/V Professor Logachev* and being able to sample the massive sulfides. Discussion with G. Tret'yakov, N. Ayupova, E. Belogub, V. Maslennikov, and V. Zaykov are greatly appreciated. This research was supported by the Russian Scientific Foundation (project no. 14-17-00691). Microprobe analysis was partially supported by Progetto di Ateneo

CPDA068444 and Progettino di Cooperazione Internazionale (Fondi PVS, 2007) of the University of Padova to P.N. P.N. also acknowledges financial support by MIUR ex60%. We gratefully acknowledge Cornel de Ronde for his detailed and constructive review, which helped us greatly to improve this paper.

FIGURE CAPTIONS

Fig. 1. (a) Geological sketch of the Central Urals (simplified after Puchkov 1993) with location of the Saf'yanovka deposit. (b) cross–section of the deposit, simplified after unpublished report of Korovko et al. (2004). (c) reconstruction of the sulfide mound, modified after Maslennikov (2006). Stars indicate sampling sites: sample KLF (left) and sample Saf007 (right).

Fig. 2. Location of the Semenov-1 and -3 hydrothermal fields within the Semenov massive sulfide cluster (after Ivanov et al. 2008; Beltenev et al. 2009).

Fig. 3. Macroscopic structures of barite-bearing ores from the Saf'yanovka deposit and massive sulfides from the Semenov-1 and Semenov-3 hydrothermal fields: (a) colloform ore, Saf'yanovka deposit, sample KLF; (b) fine-crystalline massive sulfides, Semenov-1 field, sample 186; (c) pyrite breccia, Saf'yanovka deposit, sample Saf007; (d) pyrite breccia from the Semenov-3 field, sample 284. Aggregates of barite are indicated by arrows.

Fig. 4. Morphology of barite from the Saf'yanovka deposit and Semenov-1 and -3 hydrothermal fields: (a) platy barite crystals replaced by quartz, Saf'yanovka colloform ores, sample KLF; (b) platy barite crystals (Ba) in finely crystalline groundmass of early pyrite and quartz (Py-I + Q), with a veinlet of late pyrite (Py-II), Semenov-1 field, sample 186-1; (c) massive, platy barite crystals cut by granular quartz along the deformed, locally, stylolitic (arrows) boundaries, Saf'yanovka clastic ores, sample Saf007; (d) quartz-rimmed barite rosette on a pyrite clast, Semenov-3 field, sample 284-10. Photos (a) and (c) – thin sections, transmitted light; photos (b) and (d) – polished sections, reflected light.

Fig. 5. Histograms of homogenization temperatures and salinities of fluid inclusions in barite from the Saf'yanovka colloform ores (a–b; sample KLF) and Semenov-1 fine-crystalline massive sulfides (c–d; samples 186-1 and 292-1), Saf'yanovka (e–f, sample Saf007) and Semenov-3 (g–h, sample 284) pyrite breccias.

Fig. 6. Variations of salinity vs. homogenization temperature for fluid inclusions in barite from (a) Saf'yanovka colloform ores, (b) Semenov-1 fine-crystalline massive sulfides, (c) Saf'yanovka and (d) Semenov-3 pyrite breccias..

References

Beltenev V, Ivanov V, Rozhdestvenskaya I, Cherkashov G, Stepanova T, Shilov V, Pertsev A, Davydov M, Egorov I, Melekestseva I, Narkevsky E, Ignatov V (2007) A new hydrothermal field at 13º30' N on the Mid-Atlantic Ridge. InterRidge News 16:9–10

Beltenev V, Ivanov V, Rozhdestvenskaya I, Cherkashov G, Stepanova T, Shilov V, Davydov M, Laiba A, Kaylio V, Narkevsky E, Pertsev A, Dobretsova I, Gustaitis A, Popova Ye, Amplieva A, Evrara C, Moskalev L, Gebruk A (2009) New data about hydrothermal fields on the Mid-Atlantic Ridge between 11º–14º N: 32nd cruise of R/V Professor Logatchev. InterRidge News 18:14–18

Bendel V, Fouquet Y, Auzende J-M, Lagabrielle Y, Grimaud D, Urabe T (1993) The White Lady hydrothermal field, North Fiji back-arc basin, Southwest Pacific. Econ Geol 88:2237–2245

Berkenbosch HA, de Ronde CEJ, Gemmell JB, McNeill AW, Goemann K (2012) Mineralogy and Formation of Black Smoker Chimneys from Brothers Submarine Volcano, Kermadec Arc. Econ Geol 107:1613–1633

Bertram MA, Cowen JP (1997) Morphological and compositional evidence for biotic precipitation of marine barite. J Marine Res 55:577–593

Binns RA, Scott SD, Bogdanov YA, Lisitzin AP, Gordeev VV, Gurvich EG, Finlayson EJ, Boyd T, Dotter LE, Wheller GE, Muravyev KG (1993) Hydrothermal oxide and gold-rich sulfate deposits of Franklin Seamount, Western Woodlark Basin, Papua New Guinea. Econ Geol 88:2122–2153

Binns RA, Parr JM, Gemmel JB (1997) Precious metals in barite-silica chimneys from Franklin Seamount, Woodlark Basin, Papua New Guinea. Marine Geol. 142:119–141

Bischoff JL, Rosenbauer RJ (1984) The critical point and two-phase boundary of seawater, 200–500 °C. Earth Planet Sci Lett 68:172–180

Bodnar RJ, Vityk MO (1994) Interpretation of microthermometric data for H_2O-NaCl fluid inclusions. In: De Vivo B and Frezzotti ML (Eds) Fluid inclusions in minerals: methods and applications. Pontignana-Siena, pp 117–130

Bogdanov YuA, Bortnikov NS, Vikent’ev IV, Lein AYu, Gurvich EG, Sagalevich AM, Simonov VA, Ikorskii SV, Stavrova OO, Apollonov VN (2002) Mineralogical–geochemical peculiarities of hydrothermal sulfide ores and fluids in the Rainbow field associated with serpentinites, Mid-Atlantic Ridge (36°14'N). Geol Ore Dep 44:444–473

Bogdanov YuA, Lein AYu, Sagalevich AM, Dorofeev SA, Ul’yanova NV (2006) Hydrothermal sulfide deposits of the Lucky Strike vent field, Mid-Atlantic Ridge. Geochem. Intern. 44:403–418.

Borisenko AS (1977) Study of salt composition of fluids inclusions in minerals with a criometry. Geol Geophys 8:16–28

Bortnikov NS, Krylova TL, Bogdanov YA, Vikentyev IV and Nosik LP (1997) The 14°45’N hydrothermal field, Mid-Atlantic Ridge: Fluid inclusion and sulfur isotope evidence for submarine phase separation. In: Papunen H (ed) Mineral Deposits: Research and Exploration. Where do they meet. Proc 4th Biennial SGA Meet, Turku, Finnland. Balkema, Rotterdam 353–356

Bortnikov NS, Simonov VA, Amplieva EE, Borovikov AA (2014) Anomalously high concentrations of metals in fluid of the Semenov modern hydrothermal system (Mid-Atlantic Ridge, 13°31′ N): LA-ICP-MS study of fluid inclusions in minerals. Dokl Earth Sci 456(2): 714–719

Bortnikov NS, Simonov VA, Bogdanov YuA (2004) Fluid inclusions in minerals from modern sulfide edifices: Physicochemical conditions of formation and evolution of fluids. Geol Ore Dep 46:64–75

Bortnikov NS, Vikent’ev IV (2005) Modern base metal sulfide mineral formation in the World Ocean. Geol Ore Dep 47:13–44

Butterfield DA, Massoth GJ, McDuff RE, Lupton JE, Lilley MD (1990) Geochemistry of hydrothermal fluids from Axial Seamount hydrothermal emissions study vent field, Juan de Fuca Ridge: Subseafloor boiling and subsequent fluid-rock interaction. J Geophys Res 95:12895–12921

Butterfield DA, Nakamura K-I, Takano B, Lilley MD, Lupton JE, Resing JA, Roe KK (2011) High SO_2 flux, sulfur accumulation, and gas fractionation at an erupting submarine volcano. Geology 39(9):803–806

Cazañas X, Alfonso P, Melgarejo JC, Proenza JA, Fallick AE (2008). Geology, fluid inclusion and sulphur isotope characteristics of the El Cobre VHMS deposit, Southern Cuba. Mineral Dep 43:805–824

Cherkashov G, Bel’tenev V, Ivanov V, Lazareva L, Samovarov M, Shilov V, Stepanova T, Glasby GP, Kuznetsov V (2008) Two new hydrothermal fields at the Mid-Atlantic Ridge. Marine Geores Geotechn 26:308–316

Chernyshev IV, Bortnikov NS, Chugaev AV, Golubev VN, Fouquet Y, Amplieva EE, Stavrova OO (2011) Variation scale and heterogeneity of the lead isotope composition in sulfides from hydrothermal fields of the Mid-Atlantic Ridge: Evidence from high-precision MC-ICP-MS isotopic data. Dokl. Earth Sci. 437(2): 507–512

Chuvashov BI, Anfimov AL, Soroka EI, Yaroslavtseva NS (2011) New data on age of ore-hosting sequence of the Saf’yanovka deposit, Central Urals, based on foraminifers. Dokl Earth Sci 439(2):1076–1078.

Claypool GE, Holser WT, Kaplan IR, Sakai H, Zak I (1980) The age curves of sulphur and oxygen isotopes in marine sulphates and their mutual interpretation. Chem Geol 28:199–260

Constantinou G, Govett GJS (1972) Genesis of sulphide deposits, ochre and umber of Cyprus. Trans. Inst. Min. Metall. 81:B34–B46

Cook NJ, Ciobanu CL, Pring A, Skinner W, Shimizu M, Danyushevsky L, Saini-Eidukat B, Melcher F (2009) Trace and minor elements in sphalerite: A LA-ICPMS study. Geochim Cosmochim Acta 73:4761–4791

Cowan J, Cann J (1988) Supercritical two-phase separation of hydrothermal fluids in the Troodos ophiolite Nature 333:259–261

Dahlmann A, Wallmann K, Sahling H, Sarthou G, Bohrmann G, Petersen S, Chin CS, Klinkhammer GP (2001) Hot vents in an ice-cold ocean: Indications for phase separation at the southernmost area of hydrothermal activity, Bransfield Strait, Antarctica. Earth Planet Sci Lett 193:381–394

Davis AS, Clague DA, Zierenberg RA, Wheat CG, Cousens BL (2003) Sulfide formation related to changes in the hydrothermal system on Loihi seamount, Hawai'i, following the seismic event in 1996. Can Mineral 41:457–472

Deer WA, Howie RA, Zusmann J (1962) Rock-forming minerals. Vol. 5. Non-Silicates. London, Longmans

de Ronde CEJ, Faure K, Bray CJ, Chappell DA, Wright IC (2003) Hydrothermal fluids associated with seafloor mineralization at two southern Kermadec arc volcanoes, offshore New Zealand. Miner Dep 38:217–233

de Ronde CEJ, Hannington MD, Stoffers P, Wright IC, Ditchburn RG, Reyes AG, Baker ET, Massoth GJ, Lupton JE, Walker SL, Greene RR, Soong CWR, Ishibashi J, Lebon GT, Bray CJ, Resing JA (2005) Evolution of a submarine magmatic–hydrothermal system: Brothers volcano, southern Kermadec arc, New Zealand. Econ Geol 100:1097–1133

de Ronde CEJ, Massoth GJ, Butterfield DA, Christenson BW, Ishibashi J, Ditchburn RG, Hannington MD, Brathwaite RL, Lupton JE, Kamenetsky VS, Graham IJ, Zellmer GF, Dziak RP, Embley RW, Dekov VM, Munnik F, Lahr J, Evans LJ, Takai K (2011) Submarine hydrothermal activity and gold-rich mineralization at Brothers Volcano, Kermadec Arc, New Zealand. Miner Dep 46:541–584

Duckworth RC, Knott R, Fallick AE, Ricard D, Murton BJ, Van Dover C (1995) Mineralogy and sulphur isotope geochemistry of the Broken Spur sulphides, 29° N, Mid-Atlantic Ridge. In: Parson LM, Walker CL, and Dixon DR (eds) Hydrothermal Vents and Processes. Geol Soc, London, Spec Public 87:175–190

Eickmann B, van Zuilen MA, Thorseth IH, Pedersen R, (2010) Barite chimneys from two hydrothermal sites along the slow-spreading Arctic Ridge system: Initial isotope and mineralogical results. American Geophysical Union, Fall Meeting, abstract #OS21A-1482

Fairbridge RW (1967) Phases of diagenesis and authigenesis. In: Diagenesis in Sediments. Larsen G and Chilingar GV (Eds). Elsevier, Amsterdam, pp. 19–89

Fouquet Y, von Stackelberg U, Charlou JL, Erzinger J, Herzig PM, Muehe R, Wiedicke M (1993a) Metallogenesis in back-arc environments: the Lau Basin example. Econ Geol 88:2154–2181

Fouquet Y, Wafik A, Cambon P, Mevel C, Meyer G, Gente P (1993b) Tectonic setting and mineralogical and geochemical zonation in the Snake Pit sulfide deposit (Mid-Atlantic Ridge at 23°C N). Econ Geol 88:2018–2036

Fouquet Y, Charlou J-L, Costa I, Donvall JP, Radford-Knoery J, Pellé H, Ondréas H, Lourenço N, Ségonzac M, Tivey MK (1994) A detailed study of the Lucky Strike hydrothermal site and discovery of a new hydrothermal site: Menez Gwen; preliminary results of the DIVA1 Cruise (5–29 May, 1994). InterRidge News 3(2):14–17

Frezzotti ML, Tecce F, Casagli A (2012) Raman spectroscopy for fluid inclusion analysis. J Geochem Explor 112:1–20

Fu B, Aharon P, Byerly GR, Roberts HH (1994) Barite chimneys o the Gulf of Mexico slope: Initial report on their petrography and geochemistry. Geo-Marine Lett 14:81–87.

Gieskes JM, Simoneit BRT, Brown T, Shaw T, Wang Y-C, Magenheim A (1988) Hydrothermal fluids and petroleum in surface sediments of Guaymas Basin, Gulf of California: A case study. Can Mineral 26:589–602

Glasby GP, Iizasa K, Hannington M, Kubota H, Notsu K (2008) Mineralogy and composition of Kuroko deposits from northeastern Honshu and their possible modern analogues from the Izu-Ogasawara (Bonin) Arc south of Japan: Implications for mode of formation Ore Geol Rev 34:547–560

Goodfellow WD, Blaise B (1988) Sulfide formation and hydrothermal alteration of hemapelagic sediment in Middle Valley, Northern Juan de Fuca Ridge. Can Mineral 26: 675–696

Goodfellow WD, Franklin JM (1993) Geology, mineralogy, and chemistry of sediment-hosted clastic massive sulfides in shallow cores, Middle Valley, northern Juan de Fuca Ridge. Econ Geol 88:2037–2068

Greinert J, Bollwerk SM, Derkachev A, Bohrmann G, Suess E (2002) Massive barite deposits and carbonate mineralization in the Derugin Basin, Sea of Okhotsk: precipitation processes at cold seep sites. Earth Planet Sci Lett 203:165–180

Griffith EM, Paytan A (2012) Barite in the ocean – occurrence, geochemistry and palaeoceanographic applications. Sedimentology 59(6):1817–1835

Gruen G, Weis P, Driesner T, Heinrich CA, de Ronde CEJ (2014) Hydrodynamic modeling of magmatic–hydrothermal activity at submarine arc volcanoes, with implications for ore formation. Earth Planet Sci Letters 404:307–318

Halbach P, Pracejus B, Maerten A (1993) Geology and mineralogy of massive sulfide ores from the central Okinawa Trough, Japan. Econ Geol 88:2210–2225

Halbach P, Blum N, Münch U, Plüger W, Garbe-Schönberg D, Zimmer M (1998) Formation and decay of a modern massive sulfide deposit in the Indian Ocean. Miner Deposita 33:302–309

Hanor JS (2000) Barite-celestine geochemistry and environments of formation. In: Reviews in Mineralogy & Geochemistry – Sulfate Minerals. Alpers CN, Jambor JL and Nordstrom DK (Eds). Mineral Soc America, Washington, D.C., 40, pp 193–275

Hannington MD, Scott SD (1988) Mineralogy and geochemistry of a hydrothermal silica-sulfide-sulfate spire in the caldera of Axial Seamount, Juan de Fuca Ridge. Can Miner 26:603–625

Hannington MD, Scott SD (1989) Sulfidation equilibria as guides to gold mineralization in volcanogenic massive sulfides: Evidence for sulfide mineralogy and the composition of sphalerite. Econ Geol 84:1978–1995

Hannington MD, Jonasson IR, Herzig PM, Petersen S (1995) Physical and chemical processes of seafloor mineralization at mid-ocean ridges. In: Humphris SE, Zierenberg RA, Mullineaux LS, Thomson RE (Eds.) Seafloor hydrothermal processes. Geophys Monogr 91:115–157

Hannington MD, Galley AG, Herzig PM, Petersen S (1998) Comparison of the TAG mound and stockwork complex with Cyprus-type massive sulfide deposits. In: Herzig PM, Humphris SE, Miller DJ, Zierenberg RA (eds) Proc ODP Sci Results 158:389–415

Hao Fang, Zou Huayao, Huang Baojia (2003) Natural gas generation model and its response in accumulated fluids in the Yinggehai basin. Sci China (Series D) 46(11):1103–1112

Hein JR, Zierenberg RA, Maynard JB, Hannington MD (2007) Barite-forming environments along a rifted continental margin, Southern California Borderland. Deep-Sea Res II 54:1327–1349

Hein JR, de Ronde CEJ, Koski RA, Ditchburn RG, Mizell K, Tamura Y, Stern RJ, Conrad TA, Ishizuka O, Leybourne MI (2014) Layered Hydrothermal Barite-Sulfide Mound Field, East Diamante Caldera, Mariana Volcanic Arc. Econ Geol 109:2179–2206

Herzig PM, Hannington MD, Fouquet Y, von Stackelberg U, Petersen S (1993) Gold-rich polymetallic sulfides from the Lau back arc and implications for the geochemistry of gold in sea-floor hydrothermal systems of the Southwest Pacific. Econ Geol 88:2182–2209

Holland NG (2002) The formation of an ancient gold-rich volcanogenic massive sulphide deposit: a study of the Balta-Tau deposit in the Southern Urals of Russia. PhD thesis. University of Southampton

Hou Z, Khin Z, Qu X, Ye Q, Yu J, Xu M, Fu D, Yin X (2001) Origin of the Gacun Volcanic-Hosted Massive Sulfide Deposit in Sichuan, China: Fluid Inclusion and Oxygen Isotope Evidence. Econ Geol 96:1491–1512

Ivanov VN, Beltenev VE, Stepanova TV, Lazareva LI, Smovarov ML (2008). Sulfide ores of the new hydrothermal fields at 13°31' N MAR. In: Zaykov VV, Belogub EV and Melekestseva IYu (Eds) Metallogeny of ancient and modern oceans-2008. Ore-bearing complexes and ore facies. Miass, IMin UB RAS, pp 19–22 (in Russian)

Ixer RA, Alabaster T, Pearce JA (1984) Ore petrography and geochemistry of massive sulphide deposits within the Semail Ophiolite, Oman. Trans. Min. Metall. Sect. B 93:B114–B124

Jamieson JW, Petersen S, Augustin N, Steinführer A, Escartìn J, & ODEMAR Scientific Party (2014) Seafloor massive sulfide formation on oceanic core complexes: Recent exploration of the Semyenov and Irinovskoe hydrothermal fields, Mid-Atlantic Ridge. In: Minerals of the Ocean-7 & Deep-Sea Minerals and Mining-4. St. Petersburg, VNIIOKeangeologiya, pp. 42–45

Jewell PW, Stallard RF (1991) Geochemistry and Paleoceanographic Setting of Central Nevada Bedded Barites. J Geol 99(2): 151–170

Kelley DS, Delaney JR (1987) Two-phase separation and fracturing in mid-ocean ridge gabbros at temperatures greater than 700 °C. Earth and Planetary Science Letters 83:53–56.

Krylova MA, Melekestseva IYu (2011) Raman spectroscopy of barite from the Semenov-1 hydrothermal field (13º30.87´N, Mid-Atlantic Ridge). In: Anfilogov VN (Ed) Minerals: Structure, Properties and Methods of Investigations. Miass, IMin UB RAS, pp 194–196 (in Russian)

Koroteev VA, Yazeva RG, Bochkarev VV, Moloshag VP, Korovko AV, Sheremet'ev YuS (1997) Geological position and composition of ores from the Saf'yanovka deposit, Central Urals. Yekaterinburg, IGG UB RAS (in Russian)

Kuznetsov V, Maksimov F, Zheleznov A, Cherkashov G, Bel'tenev V, Lazareva L (2011) ^{230}Th/U chronology of ore formation within the Semyenov hydrothermal district (13°31' N) at the Mid-Atlantic Ridge. Geochronometria 38(1):72–76

Lam P, Cowen JP, Popp BN, Jones RD (2008) Microbial ammonia oxidation and enhanced nitrogen cycling in the Endeavour hydrothermal plume. Geochim et Cosmochim Acta 72:2268–2286

Lang SQ, Früh-Green GL, Bernasconi SM, Butterfield DA (2013) Sources of organic nitrogen at the serpentinite-hosted Lost City hydrothermal field Geobiology 11:154–169

Lecuyer C, Dubois M, Marignac C, Gruau G, Fouquet Y, Ramboz C (1999) Phase separation and fluid mixing in subseafloor back arc hydrothermal systems; a microthermometric and oxygen isotope study of fluid inclusions in the barite-sulfide chimneys of the Lau Basin. J Geophys Res 104:911–928

Lilley MD, Butterfield DA, Olson EJ, Lupton JE, Macko SA, McDuff RE (1993) Anomalous CH_4 and NH_2^+ concentrations at an unsedimented mid-ocean-ridge hydrothermal system. Nature 364:45–47

Lilley MD, Butterfield DA, Lupton JE, Olson EJ (2003) Magmatic events can produce rapid changes in hydrothermal vent chemistry. Nature 422:878–881

Littke R, Krooss B, Idiz E, Frielingsdorf J (1995) Molecular nitrogen in natural gas accumulations: generation from sedimentary organic matter at high temperatures. AAPG Bulletin 79(3):410–430

Lüders V, Pracejus B, Halbach P (2001). Fluid inclusion and sulfur isotope studies in probable modern analogue Kuroko-type ores from the JADE hydrothermal field (Central Okinawa Trough, Japan). Chem Geol 173:45–58

Ludwig KA, Kelley DS, Butterfield DA, Nelson BK, Früh-Green G (2006) Formation and evolution of carbonate chimneys at the Lost City hydrothermal field. Geochim Cosmochim Acta 70: 3625–3645

Machel HG (2001) Bacterial and thermochemical sulfate reduction in diagenetic settings – old and new insights. Sediment Geol 140:143–175

Maslennikov VV (2006) Lithogenesis and formation of massive sulfide deposits. Miass, IMin UB RAS (in Russian)

Maslennikova SP, Maslennikov VV (2007) Sulfide chimneys of Palaeozoic black smokers on the example of the Urals. Yekaterinburg, UB RAS (in Russian)

Maslennikov VV, Maslennikova SP, Large RR, Danyushevsky LV (2009) Study of trace element zonation in vent chimneys from the Silurian Yaman-Kasy volcanic-hosted massive sulfide deposit (Southern Urals, Russia) using laser ablation-inductively coupled plasma mass spectrometry (LA-ICPMS). Econ Geol 104:1111–1141

Massoth GJ, Butterfield DA, Lupton JE, McDuff RE, Lilley MD, Jonasson IR (1989) Submarine venting of phase-separated hydrothermal fluids at Axial Volcano, Juan de Fuca Ridge. Nature 340:702–705.

McLeod CJ, Searle RC, Murton BJ, Casey JF, Mallows C, Unsworth SC, Achenbach KL, Harris M (2009) Life cycle of oceanic core complexes. Earth Planet Sci Lett 287:333–344

McClung CR, Gutzmer J, Beukes NJ, Mezger K, Strauss H, Gertloff E (2007) Geochemistry of bedded barite of the Mesoproterozoic Aggeneys-Gamsberg Broken Hill-type district, South Africa. Min Dep 42:537–549

McMurty GM, Sedwick PN, Fryer P, VonderHaar DL, Yeh H-W (1993) Unusual geochemistry of hydrothermal vents on submarine arc volcanoes: Kasuga Seamounts, Northern Mariana Arc. Earth Planet Sci Lett 114:517–528

Melekestseva IYu, Kotlyarov VA, Khvorov PV, Ivanov VN, Bel'tenev VE, Dobretsova IG (2010) Noble-metal mineralization in the Semenov-2 hydrothermal field (13°31´ N), Mid-Atlantic Ridge. Geol Ore Dep 52(8):800–810

Melekestseva IYu, Tret'yakov GA, Nimis P, Yuminov AM, Maslennikov VV, Maslennikova SP, Kotlyarov VA, Beltenev VE, Danyushevsky LV, Large R (2014) Barite-rich massive sulfides from the Semenov-1 hydrothermal field (Mid-Atlantic Ridge, 13°30.87′ N): Evidence for phase separation and magmatic input. Marine Geol 349:37–54

Mironova OF, Salazkin AN, Garanin AV (1992) Comparison of results of gas analysis of fluid inclusions by mechanical and thermal destruction. Geokhimiya 1:78–87.

Murdmaa IO (1987) Facies of oceans. Moscow, Nauka (in Russian)

Murowchick JB, Barnes HL (1986) Marcasite precipitation from hydrothermal solutions. Geochim Cosmochim Acta 50:2615–2659

Murzin VV, Varlamov DA, Yaroslavtseva NS, Moloshag VP (2010) Mineralogy and structure of barite–sulfide veins of the Saf'yanovka massive sulfide deposit. In: Popov VA (ed) Ural mineralogical collection, pp. 12–19 (in Russian)

Naumov VB, Akhmanova MV, Sobolev AV, Dhamelncourt P (1986) Application of laser Raman-microprobe to a study of gas phase of inclusions in minerals. Geokhimiya (7):1027–1034

Nehlig P (1993) Interactions between magma chambers and hydrothermal systems: oceanic and ophiolitic constraints. J Geophys Res 98 (BI1):19621–19633

Ohmoto H (1996) Formation of volcanogenic massive sulfide deposits: The Kuroko perspective. Ore Geol Rev 10:135–177

Paytan A, Mearon S, Cobb K, Kastner M (2002) Origin of marine barite deposits: Sr and S isotope characterization. Geology 30(8): 747–750.

Petersen S, Herzig PM, Hannington MD (2000) Third dimension of a presently forming VMS deposit: TAG hydrothermal field, Mid-Atlantic Ridge, 26º N. Mineral Dep 35:233–259

Petersen S, Herzig PM, Schwarz-Schampera U, Hannington MD, Jonasson IR (2004) Hydrothermal precipitates associated with bimodal volcanism in the Central Bransfield Strait, Antarctica. Miner Dep 39:358–379

Pedersen RB, Tore Rapp H, Thorseth IH, Lilley MD, Barriga FJAS, Baumberger T, Flesland K, Fonseca R, Früh-Green GL, Jorgensen SL (2010) Discovery of a black smoker vent field and vent fauna at the Arctic Mid-Ocean Ridge. Nature Communications, DOI: 10.1038/ncomms1124

Pertsev AN, Bortnikov NS, Vlasov EA, Beltenev VE, Dobretsova IG, Ageeva OA (2012) Modern sulfide deposits of the Semenov ore region (Mid-Atlantic Ridge, 13°30' N): Types of associated rocks of the oceanic core complex and their hydrothermal alteration. Geol Ore Dep 54(5):334–346

Potter RW (1977) Pressure corrections for fluid-inclusion homogenization temperatures based on the volumetric properties of the system NaCl–H_2O. US Geol Surv J Res 5:603–607

Puchkov VN (1993) Paleooceanic structures of the Urals. Geotectonics 3:18–34 (in Russian)

Rees CE, Jenkins WJ, Monster J (1978) The sulfur isotopic composition of ocean water sulfate. Geochim Cosmochim Acta 42:377–381

Roedder E (1984) Fluid inclusions. Mineral Soc America Rev Mineral 12, 646 p

Rona PA, Hannington MD, Raman CV, Thompson G, Tivey MK, Humphris SE, Lalou C, Petersen S (1993) Active and relict sea-floor hydrothermal mineralization at the TAG hydrothermal field, Mid-Atlantic Ridge. Econ Geol 88:1989–2117

Safina NP, Maslennikov VV (2009) Sequence of mineral formation in clastic ores of the Saf'yanovka volcanic-hosted copper massive sulfide deposit, the Central Urals. Geol Ore Dep 51(7):633–643

Safina NP, Ankusheva NN., Murzin VV (2012) Physico-chemical formation conditions of barite from the ore facies of the Saf'yanovka VHMS deposit, Central Urals. Litosfera 3:110–126.

Sasaki M, Iizasa K, Sawaki T (1995) Characteristics of gases in fluid inclusions from the Nurukawa Kuroko deposit and submarine sulfide deposits of the Izu–Ogasawara arc, Japan. Res Geol 45:1–10

Sato T (1977) Kuroko deposits: their geology, geochemistry and origin. Geol. Soc. London Spec. Publ. 153–161.

Scotney PM, Roberts S, Herrington RJ (2005) The development of volcanic hosted massive sulfide and barite–gold orebodies on Wetar Island, Indonesia. Miner Dep 40:76–99

Scott S (1980) Geology and structural control of Kuroko-type massive sulfide deposits. In: The Continental Crust and Its Mineral Deposits (D.W. Strangway, ed.).Geol. Assoc. Can. Spec. Pap. 20:705–740

Seal RR II (2006) Sulfur isotope geochemistry of sulfide minerals. Rev Min Geochem 61:633–677

Shadlun TN, Bortnikov NS, Bogdanov YuA, Tufar W, Muravyev K, Gurvich EG, Muravitskaya, Korina EA, Topa T (1992) Mineral composition and origin of massive sulfide ores in the Manus backarc basin (Pacific Ocean). Geol Rudn Mestorozh 34(5):3–21

Shanks WC III, Böhlke JK, Seal RR II (1995) Stable isotopes in mid-ocean ridge hydrothermal systems: interactions between fluids, minerals and organisms. In: Humphris SE, Zierenberg RA, Mullineaux LS, Thomson RE (eds) Seafloor hydrothermal processes. Geophys Monogr 91:194–221

Simonov VA, Kovyazin SV, Terenya EO, Maslennikov VV, Zaykov VV, Maslennikova SP (2006) Physicochemical parameters of magmatic and hydrothermal processes at the Yaman-Kasy massive sulfide deposit, the southern Urals. Geol Ore Dep 48(5):369–383

Smith DK, Escartín J, Schouten H, Cann JR (2008) Fault rotation and core complex formation: significant processes at slow-spreading mid-ocean ridges (Mid-Atlantic Ridge, 13°–15°N). Geochem. Geophys. Geosyst. 9. doi:10.1029/2007GC001699.

Soroka EI, Moloshag VP, Petrishcheva VG (2010) Al-bearing mineral assemblage with alunite in ore-hosting rocks of the Saf'yanovka VMS deposit, Central Urals. Litosfera 6:112–119.

Steele JH, Thorpe SA, Turekian KK (2010) Marine chemistry and geochemistry: a derivative of encyclopedia of ocean sciences. 2nd edition. London, Elsevier. 631 p.

Suzuki R, Ishibashi J-I, Nakaseama M, Konno U, Tsunogai U, Gena K, Chiba H (2006) Diverse range of mineralization Iinduced by phase separation of hydrothermal fluid: Case study of the Yonaguni Knoll IV hydrothermal field in the Okinawa Trough back-arc basin. Res Geol 58:267–288

Thompson G, Humphris SE, Schoeder B, Sulanowska M, Rona P (1988) Active vents and massive sulfides at 26° N (TAG) and 23° N (Snakepit) on the Mid-Atlantic Ridge. Can Mineral 26: 697–711

von Damm KL, Bray AM, Buttermore LG, Oosting SE (1998) The geochemical controls on vent fluids from the Lucky Strike vent field, Mid-Atlantic Ridge. Earth Planet Sci Lett 160:521–536

von Damm KL, Lilley MD, Shanks WCIII, Brockington M, O'Grady KM, Olson E, Graham A, Proskurowski G, Bray AM and the SouEPR Science Party (2003) Extraordinary phase separation and segregation in vent fluids from the southern East Pacific Rise. Earth Planet Sci Lett 206:365–378

Yapaskurt OV (2005) Aspects of postsedimentation lithogenesis theory. Lithosphere 3:3–30

Yaroslavtseva NS, Maslennikov VV, Safina NP, Leshchev NV, Soroka EI (2012) Black shales of the Saf'yanovka massive sulfide deposit, Middle Urals. Litosphere (2):106–124

Yazeva RG, Moloshag VP, Bochkarev VV (1991) Geology and ore parageneses of the Saf'yanovka massive sulfide deposit in the Central Urals back thrust. Geol Ore Dep 33(4):76–58

Zierenberg RA, Koski RA, Morton JL, Bouse RM (1993) Genesis of massive sulfide deposits on a sediment-covered spreading center, Escanaba Trough, southern Gorda Ridge. Econ Geol 88:2069–2098

Figure

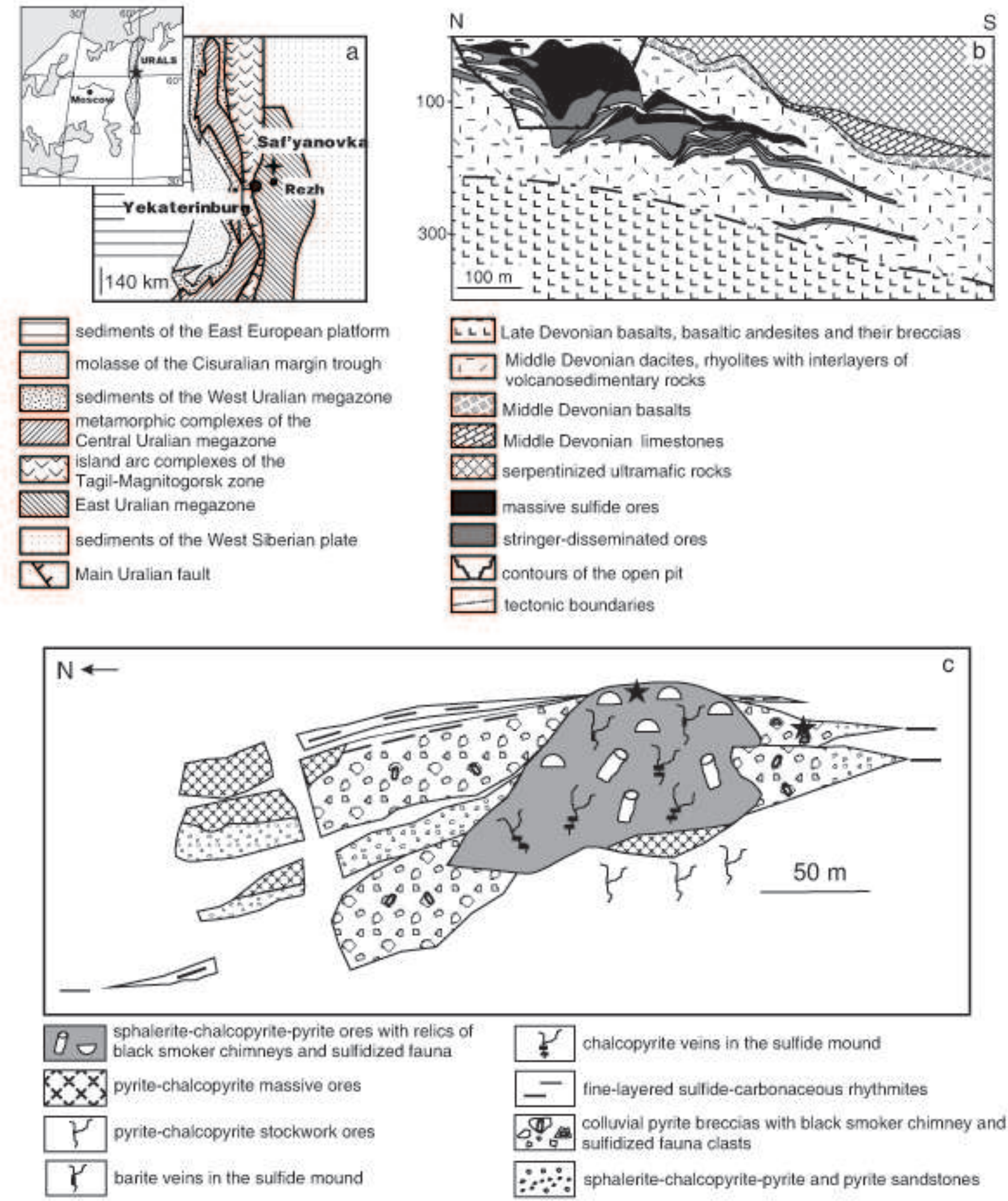
a
URALS
Moscow
Saf'yanovka
Rezh
Yekaterinburg
140 km
sediments of the East European platform
molasse of the Cisuralian margin trough
sediments of the West Uralian megazone
metamorphic complexes of the Central Uralian megazone
island arc complexes of the Tagil-Magnitogorsk zone
East Uralian megazone
sediments of the West Siberian plate
Main Uralian fault
N
S
b
100
300
100 m
Late Devonian basalts, basaltic andesites and their breccias
Middle Devonian dacites, rhyolites with interlayers of volcanosedimentary rocks
Middle Devonian basalts
Middle Devonian limestones
serpentinized ultramafic rocks
massive sulfide ores
stringer-disseminated ores
contours of the open pit
tectonic boundaries
N
c
50 m
sphalerite-chalcopyrite-pyrite ores with relics of black smoker chimneys and sulfidized fauna
pyrite-chalcopyrite massive ores
pyrite-chalcopyrite stockwork ores
barite veins in the sulfide mound
chalcopyrite veins in the sulfide mound
fine-layered sulfide-carbonaceous rhythmites
colluvial pyrite breccias with black smoker chimney and sulfidized fauna clasts
sphalerite-chalcopyrite-pyrite and pyrite sandstones

Figure

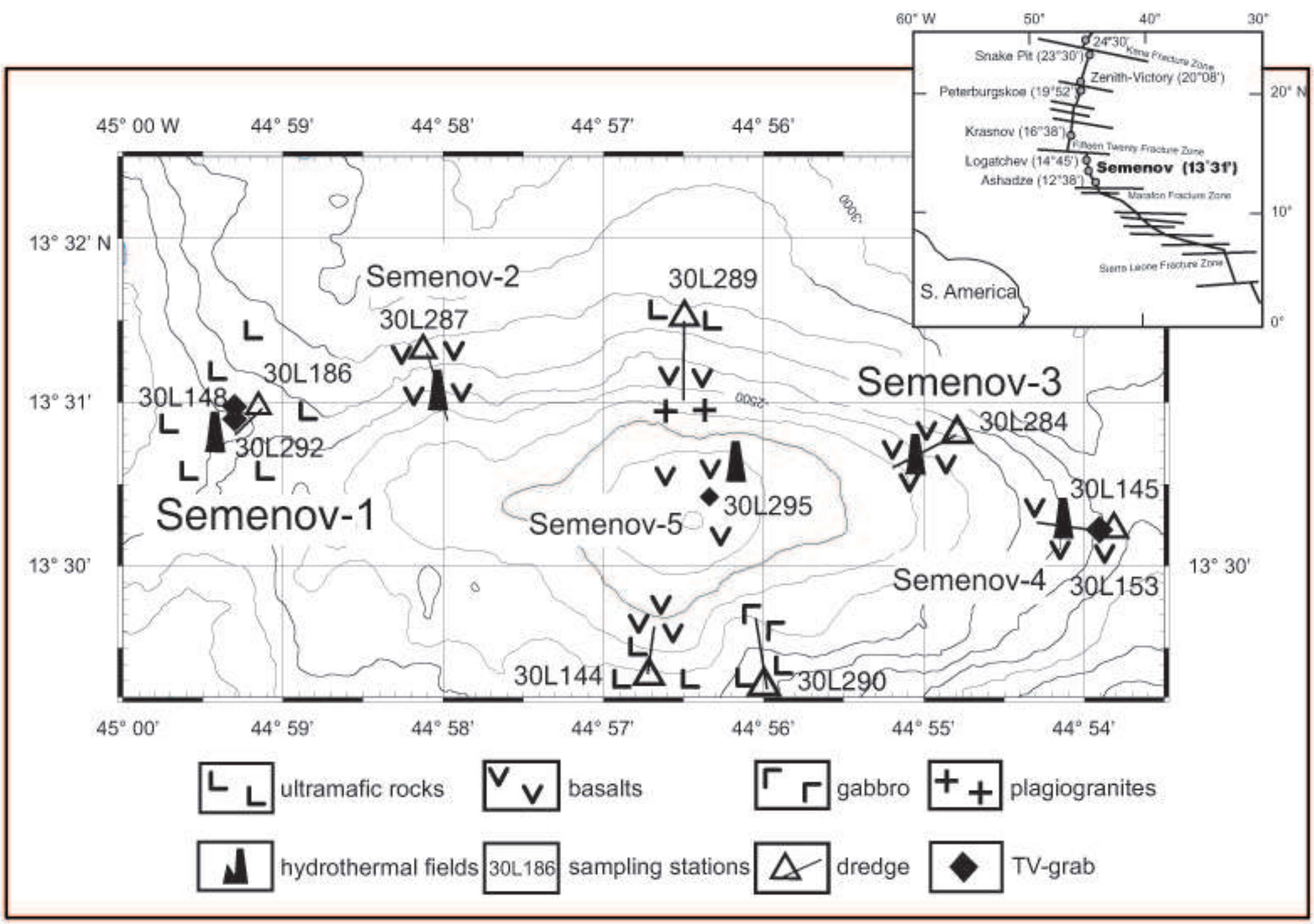

45° 00 W
44° 59'
44° 58'
44° 57'
44° 56'
13° 32' N
13° 31'
13° 30'
45° 00'
44° 55'
44° 54'
Semenov-1
Semenov-2
Semenov-3
Semenov-4
Semenov-5
30L148
30L186
30L292
30L287
30L289
30L284
30L295
30L145
30L153
30L144
30L290
3000
2500
60° W
50°
40°
30°
20° N
10°
0°
24°30'
Snake Pit (23°30')
Kane Fracture Zone
Zenith-Victory (20°08')
Peterburgskoe (19°52')
Krasnov (16°38')
Fifteen Twenty Fracture Zone
Logatchev (14°45')
Semenov (13°31')
Ashadze (12°58')
Marathon Fracture Zone
Sierra Leone Fracture Zone
S. America
ultramafic rocks
basalts
gabbro
plagiogranites
hydrothermal fields
30L186
sampling stations
dredge
TV-grab

Figure

Click here to download high resolution image

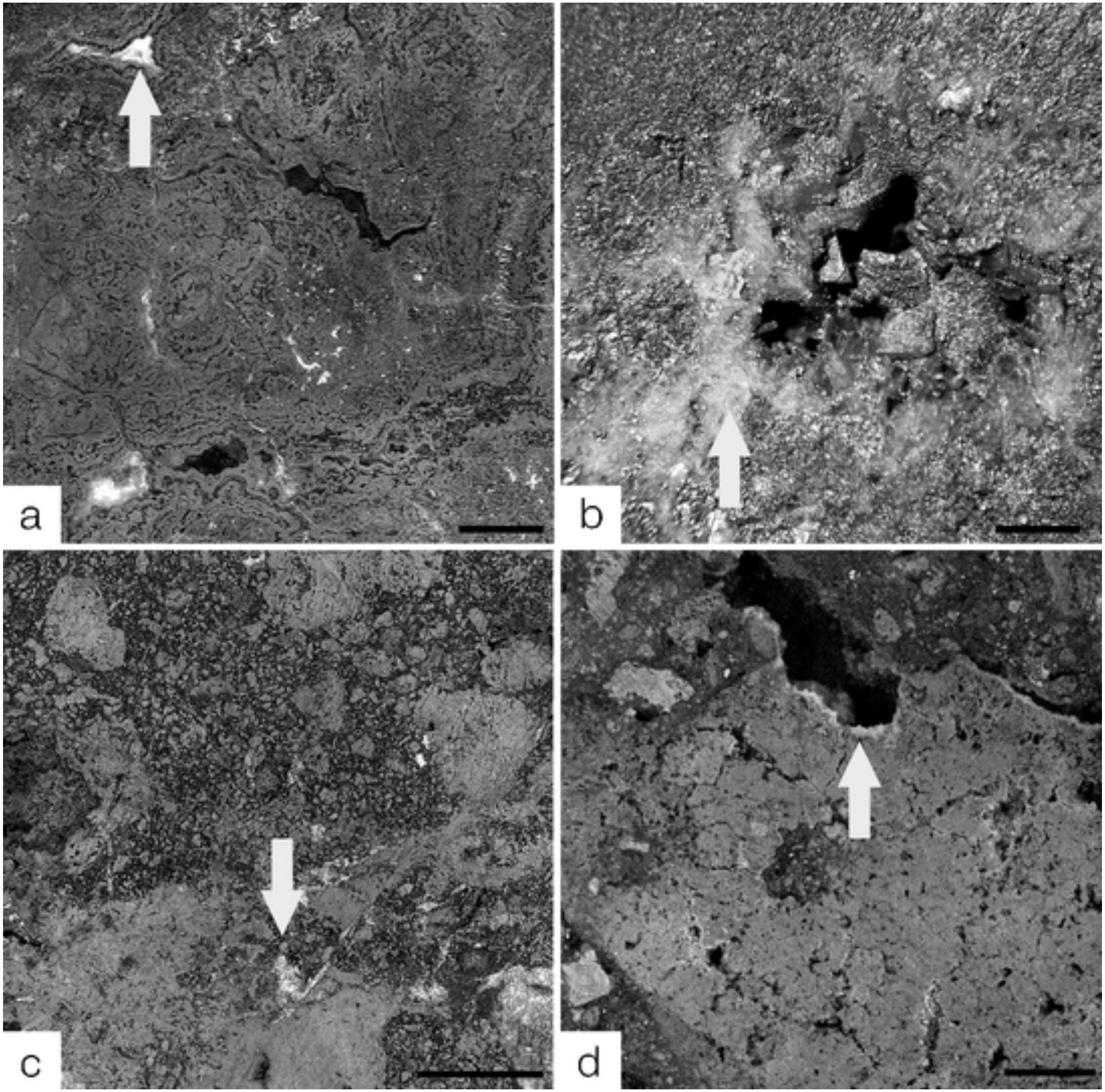

Figure
Click here to download high resolution image

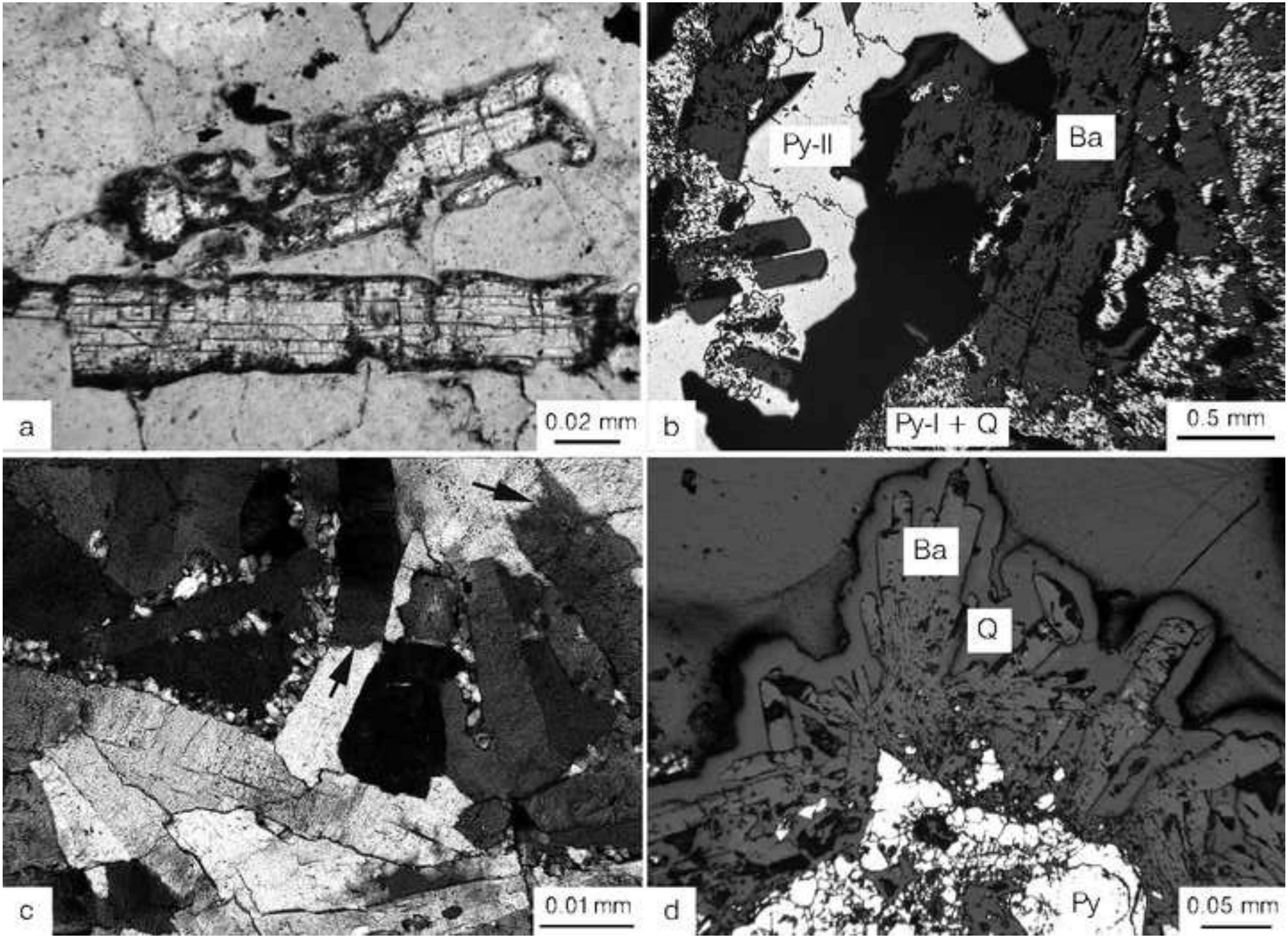

Figure

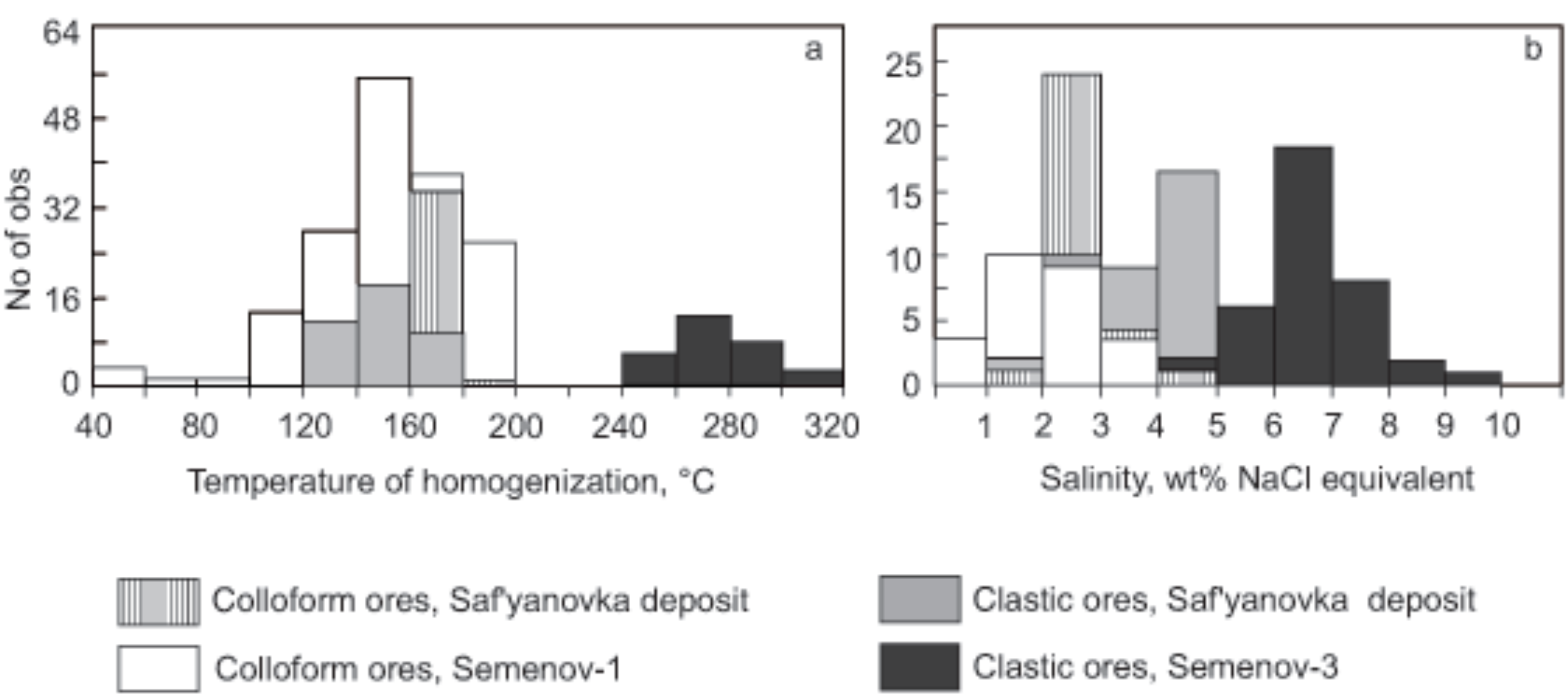

64
48
32
16
0
No of obs
a
40
80
120
160
200
240
280
320
Temperature of homogenization, °C
25
20
15
10
5
0
b
1
2
3
4
5
6
7
8
9
10
Salinity, wt% NaCl equivalent
Colloform ores, Saf'yanovka deposit
Colloform ores, Semenov-1
Clastic ores, Saf'yanovka deposit
Clastic ores, Semenov-3

Figure

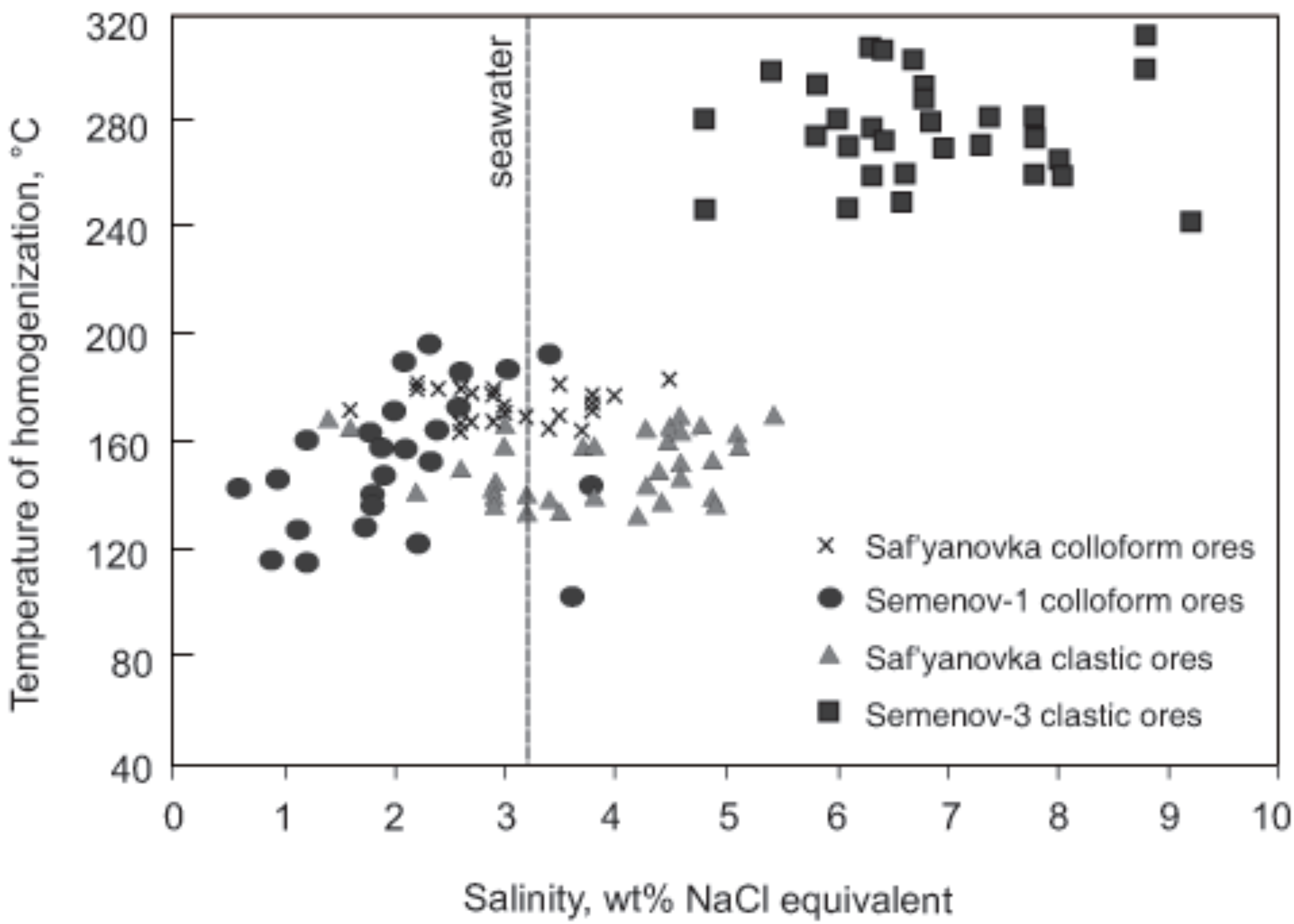

320
280
240
200
160
120
80
40
Temperature of homogenization, °C
seawater
0
1
2
3
4
5
6
7
8
9
10
Salinity, wt% NaCl equivalent
Saf'yanovka colloform ores
Semenov-1 colloform ores
Saf'yanovka clastic ores
Semenov-3 clastic ores

Table

Table 1 Coordinates of sampling stations at the Semenov-1 and -3 hydrothermal fields

Stations	Latitude		Longitude		Depth	
	Start	Finish	Start	Finish	Start	Finish
Semenov-1 field						
Dredge, st. 186	13.30.960 N	13.30.802 N	44.59.130 W	44.59.297 W	2646 m	2592 m
TV-grab, st. 292	13 30.872 N		44 59.237 W		2595 m	
Semenov-3 field						
Dredge, st. 284	13 30.801 N	13 30.601 N	44 54.800 W	44 55.195 W	2616 m	2393 m

Table

Table 2 Average electron microprobe analyses of barite, wt%

Oxides	Saf'yanovka colloform ores, sample KLF (n = 7)	Semenov-1 fine-crystalline sulfides		Saf'yanovka clastic ores, sample 007, (n = 3)	Semenov-3 clastic ores, sample 284 (n = 9)
		sample 186 (n = 5)	sample 292 (n = 8)		
BaO	65.03 (0.35)	66.61 (1.2)	61.64 (1.37)	65.06 (0.36)	64.17 (1.51)
SrO	0.57 (0.25)	1.09 (0.68)	3.41 (1.10)	0.35 (0.61)	1.74 (1.49)
SO_3	34.27 (0.34)	33.48 (0.1)	34.15 (0.61)	34.42 (0.11)	33.60 (0.51)
Total	99.89	101.26	99.25	99.83	99.18

n, number of analyses
Standard deviation is given in brackets
Barite also contains (average, wt%) 0.11 FeO (sample 292); 0.06, 0.05 PbO (samples 186, 284, respectively); 0.01, 0.02, 0.19, 0.01 CaO (samples KLF, 186, 292, 284, respectively); 0.03 and 0.04 ZnO (samples 186 and 284, respectively)

Table

Table 3 Trace element composition of barite, ppm

Elements	Colloform ores	Breccia	Fine-crystalline sulfides	Breccia
	Saf'yanovka deposit		Semenov-1 field	Semenov-3 field
	sample KLF	sample Saf007	sample 186	sample 284
Cu	142	201	89	444
Zn	171	293	235	158
Pb	15	136	16	42
Ga	n.d.	0.3	0.1	0.3
Ge	0.1	0.1	0.1	0.4
As	n.d.	2	n.d.	n.d.
Se	0.2	0.3	0.3	0.2
Cd	n.d.	0.01	0.02	1
Sn	n.d.	n.d.	2	n.d.
Sb	1	1.4	3	6
Te	0.02	0.1	0.1	0.01
Hg	n.d.	3	n.d.	n.d.
Bi	0.03	0.4	0.01	0.03
Co	0.1	0.1	32	44
Ni	15	7	335	438
Mn	1	8	34	5
Sr	2529	3095	7051	3408

n.d., not detected.

The contents of Cu, Zn, Pb, Co, Ni, Cd, As, Se, Sb, Te, Tl, Mo, V, Cr, Mn, Sr, and U for the Semenov-1 barite are taken from (Melekestseva et al., 2014).

Table

Table 4 Sulfur isotopic data ($\delta^{34}S_{CTD}$‰) for barite from the Saf'yanovka deposit and Semenov-1 and -3 hydrothermal fields

Sample	$\delta^{34}S_{CTD}$‰
Saf'yanovka deposit, colloform ores	
Klf	+25.5
Klf-1	+22.7
Klf-1a	+22.1
Klf-2a	+23.5
Klf-3	+23.2
Klf-5	+20.9
Average	*+22.9 (1.5)*
Saf'yanovka deposit, clastic ores	
Saf-007	+27.0
Saf-007-1	+28.8
Saf-007-2	+28.0
Saf-007-3	+28.4
Saf-007-4	+27.3
Saf-007-5	+29.2
Average	*+28.1 (0.9)*
Semenov-1 field, colloform ores*	
186	+21.0
292	+21.3
Average	*+21.2 (0.2)*
Semenov-3 field, clastic ores	
284-1	+20.6
284-2	+18.7
284-3	+19.1
284-4	+19.9
Average	*+19.6 (0.8)*

*, data from Melekestseva et al. 2014; standard deviation is given in brackets.

Table

Table 5 Summary of the fluid inclusion data for barite of the studied deposits

T_e, °C	Major salts in the fluids	$T_{m.}$, °C	Salinity, wt.% NaCl-eq.	T_{hom}, °C	Pressure, bar	T_f, °C
Colloform ores, Saf'yanovka deposit						
–21.7 to –22.3 (n = 6)	$NaCl–Na_2CO_3–H_2O$ ± $NaHCO_3$ and Na_2SO_4	–0.9 to –2.7 (n = 35)	1.6–4.5	162–184 (n = 35)	100 to 150	172–194
Fine-crystalline sulfides, Semenov-1 field (Melekestseva et al., 2014)						
–6.6 to –2.2 (n = 30)	$Na_2SO_4–K_2SO_4–H_2O$ and $Na_2SO_4–NaHCO_3–H_2O$	–0.5 to – 2.8 (n = 26)	0.6–3.8	58–199 (n = 180)	250	83–224
Clastic ores, Saf'yanovka deposit						
–22.0 to –22.3 (n = 7)	$NaCl–H_2O$ ± $NaHCO_3$ and Na_2SO_4	–0.8 to –3.3 (n = 44)	1.4–5.4	130–170 (n = 44)	100 to 150	140–180
Clastic sulfides, Semenov-3 field						
–21.1 to –21.8 (n = 8)	$NaCl–H_2O$	–3.0 to –6.0 (n = 31)	4.8–9.2	241–310 (n = 31)	250	266–335

T_e, eutectic temperature; T_m, final temperature of ice melting; T_{hom}, homogenization temperature; T_f, minimum temperature of formation.
Pressure estimations are described in the text.
n is the number of measurements.

Table

Table 6 Vapor composition of fluid inclusions in barite from the Saf'yanovka deposit and Semenov-3 field (mol%) in comparison with data on some hydrothermal fields and VMS deposits

Deposits	H_2O	CO_2	CO	CH_4	N_2
Saf'yanovka deposit, colloform ores	96.91	1.58	1.5	0.05	0.006
Saf'yanovka deposit, clastic ores	98.93	0.64	0.41	0.02	0.02
Semenov-3 field, clastic ores	98.10	1.60	0.30	0.01	n.d.
Brother Volcano[a]	99.979	0.013	n.d.	0.002	0.006
Rumble II West[b]	99.946	0.037	n.d.	0.002	0.006
Miojinsho[d]	99.4	0.35	n.d.	0.0027	0.048
Kita-Bayonaise[d]	99.4	0.24	n.d.	0.0042	0.045

[a]de Ronde et al. 2003, sample X573/G (barite+sulfides)
[b]de Ronde et al. 2003, sample X656/A (barite+sulfides)
[c]our calculations
[d]Sasaki et al. 1995